

CONF. 950926--1

CONF. 950926--1

CONF. 950926--1

OCTI

HYDROGEN PICKUP AND REDISTRIBUTION IN ALPHA-ANNEALED ZIRCALOY-4

B. F. Kammenzind, D. G. Franklin, H. R. Peters, and W. J. Duffin

DISCLAIMER

This report was prepared as an account of work sponsored by an agency of the United States Government. Neither the United States Government nor any agency thereof, nor any of their employees, makes any warranty, express or implied, or assumes any legal liability or responsibility for the accuracy, completeness, or usefulness of any information, apparatus, product, or process disclosed, or represents that its use would not infringe privately owned rights. Reference herein to any specific commercial product, process, or service by trade name, trademark, manufacturer, or otherwise does not necessarily constitute or imply its endorsement, recommendation, or favoring by the United States Government or any agency thereof. The views and opinions of authors expressed herein do not necessarily state or reflect those of the United States Government or any agency thereof.

BETTIS ATOMIC POWER LABORATORY

WEST MIFFLIN, PENNSYLVANIA 15122-0079

Operated for the U.S. Department of Energy
by WESTINGHOUSE ELECTRIC CORPORATION

DISTRIBUTION OF THIS DOCUMENT IS UNLIMITED

MASTER

HYDROGEN PICKUP AND REDISTRIBUTION IN ALPHA-ANNEALED ZIRCALOY-4

B. F. Kammenzind¹, D. G. Franklin¹, H. R. Peters², and W. J. Duffin¹

¹Bettis Atomic Power Laboratory
Westinghouse Electric Corporation
West Mifflin, Pennsylvania 15122

²Knolls Atomic Power Laboratory
Martin Marietta Corporation
Schenectady, New York 12301-1072

ABSTRACT: Zircaloy-4, which is widely used as a core structural material in Pressurized-Water Reactors (PWR), picks up hydrogen during service. Hydrogen solubility in Zircaloy-4 is low and hydrides precipitate after the Zircaloy-4 matrix becomes supersaturated with hydrogen. These hydrides embrittle the Zircaloy-4. To study hydrogen pickup and concentration, a postirradiation nondestructive radiographic technique for measuring hydrogen concentration was developed and qualified. Experiments on hydrogen pickup were conducted in the Advanced Test Reactor (ATR). Ex-reactor tests were conducted to determine the conditions for which hydrogen would dissolve, migrate, and precipitate. Finally, a phenomenological model for hydrogen diffusion was indexed to the data. This presentation describes the equipments and the model, presents the results of experiments, and compares the model predictions to experimental results.

KEYWORDS: Zircaloys, hydrogen, corrosion, diffusion, hydrogen redistribution, hydrogen solubility

INTRODUCTION

During service, Zircaloys pickup hydrogen, primarily from hydrogen that is liberated as part of the oxidation of Zircaloy by water (1). Hydrogen in solution will diffuse down a thermal gradient and concentrate in cold regions of Zircaloy components (2). Due to the low solubility of hydrogen in Zircaloys, zirconium hydrides form at relatively low concentrations of hydrogen, especially on cooling to near room temperature. These hydrides are brittle and at low concentration begin to degrade the mechanical properties of Zircaloys (3). These changes in properties need to be considered in component evaluations. Fundamental data and models that describe hydrogen pickup and redistribution can be used in this evaluation process. To provide the bases for such evaluations, in-reactor and out-of-reactor experiments were conducted to develop a database for a fundamental model that provides insight into the phenomena involved.

The low solubility of hydrogen in zirconium alloys and the detrimental effects of hydrides was recognized in the 1950s (4) during early development of zirconium alloys for nuclear application. Under normal conditions the influx of hydrogen in-reactor is quite low. Further, it

DISCLAIMER

This report was prepared as an account of work sponsored by an agency of the United States Government. Neither the United States Government nor any agency thereof, nor any of their employees, make any warranty, express or implied, or assumes any legal liability or responsibility for the accuracy, completeness, or usefulness of any information, apparatus, product, or process disclosed, or represents that its use would not infringe privately owned rights. Reference herein to any specific commercial product, process, or service by trade name, trademark, manufacturer, or otherwise does not necessarily constitute or imply its endorsement, recommendation, or favoring by the United States Government or any agency thereof. The views and opinions of authors expressed herein do not necessarily state or reflect those of the United States Government or any agency thereof.

diffuses rapidly in the Zircaloy matrix and the hydride does not form at the corroding surface and propagate into the metal as does the oxide. Rather hydrides precipitate heterogeneously as delta hydride, Zr_2H_3 , throughout the metal at sites that can best accommodate the seventeen-percent volume increase on formation of the hydride. Due to the protective nature of zirconium oxide, corrosion and hydrogen pickup are limited. As long as the environment is not too reducing, the only hydrogen pickup in the metal is from the corrosion process (5). Therefore, hydrogen is not a concern to clad integrity under normal operating conditions, at least until much corrosion has occurred or hydrogen has concentrated in cold regions.

One of the first modes of fuel rod failure in commercial power reactors was from hydride blisters, which consisted of a high concentration of hydrides in a local cladding region (6). Hydride blisters formed either from internal moisture in the fuel rod, e.g., moisture in the fuel-pellet open porosity, or from coolant entering through fuel-cladding defects. Hydride failures were almost eliminated in the 1970s by special drying methods for fuel pellets and by reductions in defects of other types.

Performance of Zircaloy-clad fuel rods has been excellent since 1980 (7). However, isolated instances of hydride failures have occurred. Steep local temperature gradients may have caused concentration of hydrogen in cladding on PWR fuel rods (8). These concentrations of hydrides may have been sufficient to embrittle the Zircaloy-4 metal and promote clad cracking. More recently, use of zirconium liners on fuel cladding may have promoted both hydrogen pickup in defected fuel rods, due to the relatively poor corrosion resistance of zirconium liners, and high stresses from the liner volume expansion as it oxidizes (9-11). An intermediate step may be the preferential hydride formation in the zirconium liner over that of the adjacent Zircaloy-2, despite the higher liner temperature, due to the lower strength of the liner (Figure 14 of Reference 10). Hydrides form preferentially in regions of low strength due to the volume expansion during hydride formation (12). This expansion may increase stresses in the Zircaloy-2 prior to full liner oxidation. Subsequent oxidation of the liner removes evidence of this step. This failure mode illustrates the complicated nature and importance of hydrogen diffusion and hydride formation. Understanding hydrogen behavior becomes more important as fuel burnups are increased, which results in increased corrosion and hydrogen pickup (13).

Fundamental experiments and modeling of diffusion kinetics were reported during early development of zirconium alloys for nuclear applications. Appropriate references are provided below in the discussion of the results presented herein. Recent work primarily addressed hydrogen in Zr-2.5Nb pressure tubes, as reported by Canadian researchers (5, 14-

17). These experiments are characterized by studies by hydrogen concentration profiles rather than bulk hydrogen pickup measurements. Little recent work on Zircaloys has been reported. These data and associated models are required to predict the pickup, movement, and precipitation of hydrogen. As shown by the discussion above on the impact of hydrogen on fuel performance, such a capability is important if it can be used to avoid designing and operating fuel elements in a region where large concentrations of hydrides and stresses develop.

Hydrogen Pickup

Experimental

Hydrogen pickup was measured on alpha-annealed Zircaloy-4 coupons that were irradiated in the Advanced Test Reactor (ATR) at 310°C (590°F) and 360°C (680°F). A hydrogen overpressure is maintained in the cooling water to control the oxygen level in the coolant. Under normal conditions this molecular hydrogen does not act as a hydrogen source as the oxide film is essentially impervious to the molecule. The source of the hydrogen entering the Zircaloy is that produced in the corrosion reaction. A nondestructive method of measuring hydrogen content was developed and qualified. This method measured the neutron attenuation by absorbed hydrogen as a neutron beam passed through a specimen (Figure 1). A neutron beam with a white noise spectrum was filtered by passing it through indium-cadmium material. This removed most neutrons with energies that activated indium atoms, resulting in the spectrum shown in Figure 1 as the incident notched spectrum. Passing this beam through a thin foil of indium (in Detector (D_1) in Figure 1) activated this foil in proportion to the remaining number of neutrons at the indium activation energies. This foil was counted to produce the signal value D_1 . The neutron beam then passed through the Zircaloy-4 sample. The neutrons interacted with hydrogen atoms in the Zircaloy-4, which reduced the energy of many of the neutrons. This neutron scattering resulted in many neutrons having their energies decreased to the energy bands for indium activation. This new neutron beam energy spectrum is shown in Figure 1 as the moderated notched spectrum. The moderated beam passed through another indium foil (in detector (D_2) in Figure 1) and activated the indium in proportion to the numbers of neutrons at the indium energies. This foil was counted to determine D_2 . The relative difference between D_2 and D_1 was proportional to the amount of hydrogen in specimen, $(D_2 - D_1) / D_1$. The attenuation of the beam was calibrated to the hydrogen content of Zircaloy-4 by the use of standards. In addition, each set of specimens included a standard with a known concentration of hydrogen. Since the method was nondestructive, interim measurements were made on coupons using an on-site neutron beam. This allowed the hydrogen pickup of individual samples to be followed as a function of radiation exposure. Out-of-reactor

hydrogen pickup was measured after autoclave exposure by destructive hot vacuum extraction to obtain reference data.

Results

Out-of-reactor reference pickup data Zircaloy-4 coupons from three ingots are shown in Figure 2 for 316°C exposure. Autoclave water was degassed and deionized at pH 7 with a resistivity above 1 million ohm centimeters. Pressure was held above that for saturation at 316°C, about 10.65 MPa. Similar in-reactor pickup data are shown in Figures 3 and 4 for exposure at 360°C and 310°C, respectively, for three neutron flux levels: high flux or $\phi > 10^{18}$ n/m²/sec, medium flux or 10^{18} n/m²/sec $> \phi > 10^{17}$ n/m²/sec, and low flux or $\phi < 10^{17}$ n/m²/sec. The data are listed in Table 3 for autoclave exposures, and Table 4 for in-reactor exposures. Table 5 lists the chemistry of the Zircaloy-4 used in the testing. To determine if the hydrogen pickup was correlated with sample oxidation, the measured hydrogen content was plotted as a function of measured oxygen concentration, as determined by weight-gain measurements and as shown in Figure 5. This suggested that most of the hydrogen absorbed during service was from the oxidation. Further, it supported use of a factor to estimate hydrogen pickup from measured or predicted oxidation. In general, the hydrogen pickup is correlated to the oxidation. Above 1000 (mg/sq dm) the pickup ratio ($\Delta H/\Delta O$) tends to deviate in both directions from the average value. This is due to a sensitivity of the hydrogen pickup ratio ($\Delta H/\Delta O$) to temperature and fluence as suggested in Figure 6.

Hydrogen Content of Oxide Films

Experimental

The hydrogen concentration in the oxide film may be different from the hydrogen concentration in the Zircaloy-4 metal. Several studies have shown this to be the case (14, 18). High or low hydrogen concentrations in the oxide can have an impact on interpretation of hydrogen measurements to determine $\Delta V/\Delta O$ ratios and hydrogen migration. To determine the impact of this effect, Secondary Ion Mass Spectroscopy (SIMS) was used to determine the concentration distribution through the oxide and metal of an autoclave Zircaloy-4 specimen. The hydrogen distribution is shown in Figure 7, in which hydrogen is uniformly dispersed in the oxide and concentrated in hydrides in the metal.

To quantify the hydrogen concentrations in the oxide and metal, autoclaved and in-reactor corrosion coupons were tested for hydrogen concentration, with and without the

*All fluxes are for E > 1 MeV.

oxide film, as shown in Figure 8. The oxide was removed with silicon carbide paper or with a Dremel tool. Both were used under flowing water to avoid heating the material. The results from autoclave specimens, tested at 360°C, 19.2MPa in deionized degassed water, are given in Table 1. The results from in-reactor testing are shown in Figure 9 and 10. Out-of-reactor samples exhibited similar hydrogen concentrations in the oxide and metal. However, in-reactor samples had hydrogen concentrations in the oxide much greater than that in the metal. Figures 9 and 10 show how the in-reactor hydrogen concentrations in the oxide varied with fast fluence (> 1 Mev) and oxide thickness. There is considerable scatter in both and no sign of a simple dependence of thickness, fluence, or fast flux. The hydrogen content of the oxide saturated quickly and thereafter was independent of oxide thickness, fluence, or flux. The original coupon thickness was about 1000 μm . Since the hydrogen concentration in the oxide in-reactor after about 20 μm of oxide was independent of exposure and oxide thickness (Figures 9 and 10), the relative amounts of hydrogen in the oxide and metal depended on the relative volumes of oxide and hydride as well as the amount in the metal, which does depend on exposure. In thin coupons the hydrogen in the oxide can be a significant fraction of the total hydrogen content of the oxidized coupon.

Hydrogen Migration in Zircaloy-4

Hydrogen migration down temperature gradients results in a concentration of hydrogen in hydrides when the metal hydrogen concentration exceeds solubility in the cold regions of a zirconium alloy. However, hydrogen migration models can not be based on equilibrium, principally because volume mismatch between metal and hydride densities results in lattice distortion on precipitation. The energy required to induce this distortion delays precipitation until the metal hydrogen concentration exceeds the equilibrium concentration. A model for the migration of hydrogen in Zircaloy (27), modified to accommodate a difference in the solubility limits for dissolution and precipitation of the hydride, was used to describe the process. The metal concentration at equilibrium between metal and hydrides was used for dissolution of the hydrides, C_{eq} . Precipitation of hydrides requires a supersaturation of hydrogen relative to a solubility limit for precipitation C_{PT} , which is somewhat higher than C_{eq} . When the hydrogen concentration in solution in the metal is between C_{eq} and C_{PT} , hydride will not precipitate and existing hydrides will not grow. Hydrides dissolve in equilibrium with the metal matrix at the equilibrium concentration C_{eq} . The model is summarized in Table 2. Qualification experiments were designed to confirm the model and to provide data for indexing constants.

Experimental

To determine the solid-solution diffusion coefficient, diffusion couples were made by precharging half of the sample (Figure 11) and then annealing the sample at temperatures between 260°C and 482°C, for 3.9 days at 427°C (Figure 12). The material used was that of ingot B in Table 5. Specimens were precharged with hydrogen by gaseous equilibration when the desired hydrogen distribution was uniform. Specimens where only a portion was to be precharged were cathodically precharged by partial immersion in 1N sulfuric acid, poisoned against hydrogen recombination with 0.25 grams per liter of sodium arsenate. The current was 100 ma/cm² and the temperature was 80°C.

Results

The diffusion coefficients determined from these studies are shown in Figure 13, and are in reasonable agreement with the results of Kearns (19) but below results reported by Somemo (20), Sawatzky (21, 26), and Mallett and Albrecht (22). Data in the literature have demonstrated that a hysteresis exists in the precipitation and dissolution solvi (Figure 14).

Hydrogen Dissolution

Experimental

To determine the hydride dissolution solvus, similar diffusion couples were made but the two sides were allowed to come to equilibrium at each temperature (Figure 15). The hydride dissolution solvus as a function of temperature was determined by measuring the postanneal hydrogen concentration of the initially uncharged half of the samples.

Results

The results are shown in Figure 16 and compared to the results of other researches. The results agree well with those of Sawatzky (21), Slattery (23), and Kearns (24) who used two different techniques. They do not agree with the results of Erickson and Hardie (25). Based on the agreement of three investigators, it is concluded that the data presented herein accurately reflect dissolution of zirconium hydrides in Zircaloy. In addition, there appears to be no difference between the dissolution solvi for Zircaloy-2 and Zircaloy-4.

Hydrogen Precipitation

Experimental

To determine the hydride precipitation solvus, uniformly-hydrogen-charged specimens were annealed in a temperature gradient that varied linearly and monotonically from one end of each sample to the opposite end (Figure 17). Hydrogen precharge levels were chosen such that the entire sample was in the single-phase state at the beginning of the test. The cold ends of each sample were held at either 260°C, 316°C, 371°C, or 427°C and the

temperature gradients were either 6.6°C/mm or 8.7°C/mm. Hydrogen diffuses down the temperature gradient until the concentration gradient provides sufficient counter driving force to balance the thermal migration. At equilibrium the hydrogen concentration in solution in the Zircaloy matrix will have the distribution

$$C(T) = C_0 \exp(Q^*/RT(x)).$$

This will be the temperature and spatial distribution, as $T = T(x)$, of the total or measured concentration when the total concentration is below that required for precipitation of the hydride. When the total concentration is above $C(T)$ there has been precipitation. For example, the hydrogen concentration profile when a profile close to $C(T)$ has developed except at the cold end is shown in Figure 18. In this case, the hydrogen concentration at the cold end of the specimen is well above $C(T)$, indicating precipitation. The concentration C_{eq} for dissolution of the hydride is also shown by the dashed line, which at 371°C is well below that for precipitation, C_{PT} .

Results

The results from each test are shown in Figure 19, where they are compared with literature data. At temperatures above 316°C there is reasonable agreement among the results of the three literature references and the data reported herein. Our data may have a slightly lower slope. At 260°C the precipitation concentration reported herein is greater than that reported by Erickson and Hardie or by Slattery.

Discussion

The heat of transport, Q^* in equation 1 in Table 2, was determined for each sample from the slopes of $\log([H])$ vs inverse temperature, as shown in Figure 18 for a sample with a cold end at 371°C. The results are shown in Figure 20. The reprecipitation constant, α in equation 2 in Table 2, determines the reprecipitation kinetics in this model and can be determined by measuring the surface and midplane precipitated hydrogen concentration, as shown in Figure 21. Samples were corroded in concentrated lithiated water at temperatures between 288°C and 360°C in autoclaves at pressures high enough to maintain temperature below the saturation temperature, 2.79 MPa and 18.65 MPa, respectively. The results are shown in Figure 22.

This model for hydrogen diffusion was benchmarked to several out-of-reactor experiments. One sample (Figure 23) was placed in a steep temperature gradient and the other sample (Figure 24) was placed in a shallow temperature gradient. After annealing, the

samples were sectioned and hydrogen concentrations were measured by hot vacuum extraction. The resulting hydrogen-concentration profiles are shown in Figures 23 and 24, along with the temperature profiles and the model predictions of the hydrogen concentrations. The model predicts the observed concentrations adequately for the sample with the steep temperature gradient (Figure 23) but not for the sample with the shallow temperature gradient, for which the model over predicts hydrogen concentration in the colder regions. The most likely cause of the model misprediction is hydrogen trapping at lattice defects or a second phase. Trapping would result in higher required driving forces, i.e., thermal gradients, to redistribute the hydrogen.

For application to fuel designs, the above migration model must be combined with a model for hydrogen pickup. Based on the discussion in the previous section, the pickup model must properly reflect the relative amounts of hydrogen in the metal and oxide.

Conclusions

To describe the embrittlement of zirconium alloys due to formation of hydrides, the following aspects must be understood: hydrogen pickup rate, holdup of hydrogen in the oxide, diffusion rates in a matrix with hydrogen traps, hydrogen concentration in the metal for hydride dissolution, and metal hydrogen concentration for hydride precipitation and dissolution. The experiments described provide qualification data for each aspect, although additional data are needed in some areas, e.g., no holdup of hydrogen in the oxide. The model described is adequate for steep gradients but overpredicts hydrogen redistribution for shallow temperature gradients. This deficiency is thought to be due to the lack of a description of hydrogen trapping at lattice defects, i.e., the model should reflect the binding energies between the hydrogen strain field and lattice defect strain fields.

References

1. Cox, B, "Oxidation of Zirconium and Its Alloys", Advances in Corrosion Science and Technology, Volume 5, 1976, pp. 173-391.
2. Markowitz, J. M., "The Thermal Diffusion of Hydrogen In Alpha-Delta Zircaloy-2", Trans. Met. Soc. AIME, 221 (1961), 819-824.
3. Kreyns, P. H. Bourgeois, W. F., Charpentier, P. L., White, C. J., Kammenzind, B. F., and Franklin, D. G., "Lifetime Embrittlement of Reactor Core Materials", WAPD-T-3046, ASTM STP (published elsewhere in this STP).
4. Mudge, W. L. Jr., "Effect of Hydrogen on the Embrittlement of Zirconium and Zirconium Tin Alloys", Zirconium and Zirconium Alloys, pub. Am. Soc. for Metals, Cleveland, Ohio, 1953, pp. 146-167.

5. Elmoselhi, M. B., Warr, B. D., and McIntyre, S., "A Study of the Hydrogen Uptake Mechanism in Zirconium Alloys," Zirconium In the Nuclear Industry, Tenth International Symposium, ASTM STP 1245, A.M. Garde and E. R. Bradley, Eds., American Society for Testing and Materials, Philadelphia, PA, USA, 1994 pp. 62-79.
6. Proebstie, R. A., et al., "The Mechanism of Defection of Zircaloy-Clad Fuel Rods by Internal Hydriding", Proceedings of Joint Topical Meeting on Commercial Nuclear Fuel Technology Today, Toronto, Canada, April 28-30, 1975, 75-CNA/ANS-100, pp. 2-15 to 2-34
7. Preble, E. A. et. al., "Fuel Performance Annual Report for 1990", Pacific Northwest Laboratory, Richland, WA 99352, USA, NUREG/CR-3950, PNL-5210, v.8, Nov. 1993.
8. R. Yang, O. Ozer, and H. H. Klepfer, "Fuel Performance Evaluation for EPRI Program Planning", International Topical Meeting on LWR Fuel Performance, Avignon, France, 4/21-24/91, pp. 2-58, to 2-71.
9. Schrire, David et. al, "Secondary Defect Behavior in ABB BWR Fuel", Proceedings of the 1994 International Meeting on Light Water Reactor Fuel Performance, West Palm Beach, FL, USA, April 17-21, 1994, pp. 398-409.
10. Armijo, J. S., "Performance of Failed BWR Fuel", Proceedings of the 1994 International Meeting on Light Water Reactor Fuel Performance, West Palm Beach, FL, USA, April 17-21, 1994, pp. 410-422.
11. Yang, Rosa L, et al., "EPRI Failed Fuel Degradation R&D Program", Proceedings of the 1994 International Meeting on Light Water Reactor Fuel Performance, West Palm Beach, FL, USA, April 17-21, 1994, pp. 435-446.
12. Puls, M. P., "Effects of Crack Tip Stress States and Hydride-Matrix Interaction Stresses on Delayed Hydride Cracking", Metallurgical Transactions A, 21A, (1990) pp. 2905-2917
13. Baur, Karl, et al., "Fuel Behavior in High Performance PWRs", Proceedings of the 1994 International Meeting on Light Water Reactor Fuel Performance, West Palm Beach, FL, USA, April 17-21, 1994, pp. 22-30.
14. Warr, B. D., et al., "Oxide Characteristics and their Relationship to Hydrogen Uptake in Zirconium Alloys", Zirconium in the Nuclear Industry, Ninth International Symposium, ASTM STP 1132, C. M. Eucker and A. M. Garde, Eds., American Society for Testing and Materials, Philadelphia, PA, USA, 1991, pp. 740-756.
15. Laursen, T., et al., "Hydrogen Ingress into Oxidized Zr-2.5Nb", J. Nucl. Mater., 209, (1994) pp. 52-61.
16. Laursen, T., Leslie, J. R., and Tapping, R. L., "Corrosion of Zr-2.5 wt% Nb Pressure Tube Material in D₂O Steam: Deuterium Depth Distributions Measured by Nuclear Reaction Analysis", J. Nucl. Mater., 182, (1991) pp. 151-157.
17. Laursen, T., Leslie, J. R., and Tapping, R. L., "Deuterium Depth Distributions in Oxidized Zr-2.5 wt % Nb Measured by Neutron Reaction Analysis, Journal of the Less-Common Metals, 172-174, (1991) pp. 1306-1312.

18. Woolsey, I. S. and Morris, J. R., "A Study of Zircaloy-2 Corrosion In High Temperature Water Using Ion Beam Methods", Paper #178, presented at the March 3-7, 1980 Conference of the NACE, Chicago, ILL., also in Corrosion 37 (1981), pp. 575-585.
19. Kearns, J. J., "Diffusion Coefficient of Hydrogen in Alpha Zirconium, Zircaloy-2, and Zircaloy-4", J. Nucl. Mater., 43 (1972) pp. 330-338.
20. Someno, M., "Determination of the Solubility and Diffusion Coefficient of Hydrogen in Zirconium", Nihon Kinzoku Gakkaishi 24 (1960) pp. 249-253.
21. Sawatzky, A., "The Diffusion and Solubility of Hydrogen in the Alpha Phase of Zircaloy-2", J. Nuclear Mater. 2, (1960) pp. 62-68.
22. M. W. Mallet and W. M. Albrecht, "Low Pressure Solubility and Diffusion of Hydrogen in Zirconium", J. Electrochemical Soc., 104 (1957) pp. 142.
23. Slattery, G. F., "The Terminal Solubility of Hydrogen in Zirconium Alloys between 30 and 400°C", J. Inst. Metals, 95 (1967) pp. 43-47.
24. Kearns, J. J., "Terminal Solubility and Partitioning of Hydrogen in the Alpha Phase of Zirconium, Zircaloy-2 and Zircaloy-4", J. Nuclear Mater. 22 (1967) pp. 292-303.
25. Erickson, W. H. and Hardie, D., "The Influence of Alloying Elements on the Terminal Solubility of Hydrogen in α -Zirconium", J. Nuclear Mater. 13 (1964) pp. 254-262.
26. Sawatzky, A. and Wilkins B.J.S., "Hydrogen Solubility in Zirconium Alloys Determined by Thermal Diffusion", J. Nuclear Mater. 22 (1967) pp. 304-310.
27. Marino, G. P., "A 2-Dimensional Computer Program for Migration of Interstitial Solutes of Finite Solubility in a Thermal Gradient", WAPD-TM-1157, June 1974.
28. Marino, G. P., "Hydrogen Supercharging in Zircaloy", Mater. Sci. Eng., 7 (1971) pp. 335-341.

Acknowledgement

This work was supported by DOE contract DE-AC11-93PN38195.

NOTICE

This report was prepared as an account of work sponsored by the United States Government. Neither the United States, nor the United States Department of Energy, nor any of their employees, nor any of their contractors, subcontractors, or their employees, makes any warranty, express or implied, or assumes any legal liability or responsibility for the accuracy, completeness or usefulness of any information, apparatus, product or process disclosed, or represents that its use would not infringe privately owned rights.

TABLE 1 - Hydrogen Retained in Oxide Autoclaves Samples

Sample	Sample Thickness	Wt. Gain	Hydrogen Content (ppm)	
			Oxide On*	Oxide Off**
1	890 μm	642 mg/dm ²	669 \pm 11	660 \pm 7
2	890 μm	616 mg/dm ²	751 \pm 9	750 \pm 4
3	1,550 μm	1091 mg/dm ²	574 \pm 8	589 \pm 6
4	1,450 μm	993 mg/dm ²	558 \pm 10	552 \pm 6
5	1,650 μm	204 mg/dm ²	177 \pm 3	185 \pm 6
6	2,890 μm	1052 mg/dm ²	337 \pm 3	338 \pm 3

*Measurements of hydrogen concentration in both metal and oxide.

**Measurements of hydrogen concentration in metal only.

TABLE 2 - Model Used for the Migration of Hydrogen

- I. Hydrogen diffuses through the alpha (hcp) phase in response to temperature and solid solution concentration gradients.

$$\vec{J} = -D\nabla C - \frac{DQ^*C}{RT^2} \nabla T$$

D - Diffusion coefficient of hydrogen through α Zircaloy

C - Solid solution concentration of hydrogen in α Zircaloy

Q^* - Heat of Transport

T - Temperature

- II. The rate of change in hydrogen concentration at a point is

$$\frac{\delta C_T}{\delta t} = -\nabla \cdot J$$

The rate of change in hydrogen concentration solid solution in the α Zircaloy is

$$\frac{\delta C}{\delta t} = -\nabla \cdot J - \alpha^2(C - C_{PT}) , C > C_{PT}$$

$$\frac{\delta C}{\delta t} = \frac{\delta C}{\delta t} = -\nabla \cdot J , C < C_{PT}, \text{ or}$$

$$\frac{\delta C}{\delta t} = 0, C = C_{eq} \text{ if hydrides are dissolving.}$$

C_T = total hydrogen concentration

C_{PT} = $C_{PT0} \exp(-Q_p/RT)$ concentration for precipitation

C_{eq} = $C_{eq0} \exp \exp(-Q_{eq}/RT)$ concentration for dissolution

α^2 = $\alpha_0^2 \exp(-2Q_e/RT)$ fitted rate parameter for precipitation

TABLE 3 - Weight Gain of Alpha-Annealed Zircaloy-4 Exposed at
316°C (589°K) in Autoclave (mg/dm sq)*

SPEC	INGOT	DAYS	O-WTGN	H-WTGN	H/O
1	A	1470.0	95.30	5.60	0.0588
2	A	854.0	49.70	2.30	0.0463
3	A	910.0	52.60	2.40	0.0456
4	A	1078.0	63.20	2.80	0.0443
5	A	266.0	21.10	0.90	0.0427
6	A	1276.0	76.70	3.30	0.0430
7	A	798.0	48.00	2.00	0.0417
8	A	1470.0	95.00	3.90	0.0411
9	A	742.0	47.10	1.90	0.0403
10	A	154.0	18.30	0.70	0.0383
11	A	350.0	26.00	1.00	0.0385
12	A	686.0	40.50	1.50	0.0370
13	A	2267.0	155.40	5.50	0.0354
14	A	518.0	27.90	1.10	0.0394
15	A	1694.0	111.40	3.50	0.0314
16	B	742.0	38.30	1.70	0.0444
17	B	910.0	52.90	2.10	0.0397
18	B	266.0	23.10	0.90	0.0390
19	B	1694.0	116.40	4.50	0.0387
20	B	854.0	52.00	2.00	0.0385
21	B	1078.0	62.60	2.40	0.0383
22	B	798.0	48.20	1.80	0.0373
23	B	1276.0	81.90	3.00	0.0368
24	B	1470.0	97.50	3.40	0.0349
25	B	518.0	29.00	1.00	0.0345
26	B	1470.0	97.60	3.30	0.0338
27	B	154.0	21.30	0.70	0.0329
28	B	350.0	28.10	0.90	0.0320
29	B	2267.0	150.70	4.60	0.0305
30	C	910.0	53.90	2.10	0.0390
31	C	1470.0	92.30	3.80	0.0390
32	C	1078.0	60.70	2.30	0.0379
33	C	798.0	49.20	1.80	0.0366
34	C	1470.0	91.50	3.40	0.0372
35	C	1694.0	106.90	4.00	0.0377
36	C	2267.0	147.70	5.40	0.0366
37	C	350.0	24.10	0.90	0.0359
38	C	742.0	47.30	1.70	0.0359
39	C	854.0	51.20	1.80	0.0352
40	C	154.0	20.30	0.70	0.0345
41	C	266.0	24.20	0.80	0.0331
42	C	518.0	30.00	1.00	0.0333
43	C	1276.0	76.70	2.30	0.0300

*Surface initially etched

TABLE 4 - Weight Gains (mg/dm sq) of Alpha-Annealed Zircaloy-4
Exposed in the Advanced Test Reactor

SPEC	INGOT	FILM	DAYS	360°C (633.1 K)					
				AVFLUX	FLUENCE	O-WTGN	H-WTGN	H/O	AVTEMP (K)
1	B	11.18	71.7	0.539	3.3	50.4	1.1	0.0218	630.4
2	B	11.17	886.2	0.760	58.2	1010.6	21.4	0.0212	626.5
2	B	11.17	723.8	0.782	48.9	814.3	17.0	0.0209	626.9
2	B	11.17	412.1	0.797	28.4	445.1	9.0	0.0202	626.3
3	B	10.35	71.7	0.873	5.4	54.8	1.3	0.0237	630.9
4	B	10.76	886.2	1.261	96.6	1326.4	26.1	0.0197	627.6
5	B	11.18	412.1	1.199	42.7	547.2	12.8	0.0234	629.8
5	B	11.18	558.6	1.261	60.9	773.5	23.7	0.0308	628.9
6	B	0.00	71.7	0.539	3.3	59.8	1.0	0.0167	630.4
7	B	0.00	71.7	0.873	5.4	63.7	2.0	0.0314	630.9
8	C	11.59	412.1	1.199	42.7	492.0	15.2	0.0308	629.6
8	C	11.59	558.6	1.261	60.9	701.4	23.4	0.0334	628.9
9	C	11.59	886.2	1.261	96.6	1209.6	28.1	0.0232	627.8
10	L	1.65	481.5	0.024	1.0	262.5	1.9	0.0074	630.9
11	C	11.59	886.2	0.760	58.2	933.9	21.3	0.0228	626.5
11	C	11.59	723.8	0.782	48.9	749.0	19.5	0.0280	626.9
11	C	11.59	412.1	0.797	28.4	409.9	7.6	0.0185	626.3
12	L	1.24	481.5	1.224	50.9	605.2	11.1	0.0183	626.7
13	D	10.35	886.2	0.760	58.2	1008.6	20.1	0.0199	626.5
13	D	10.35	723.8	0.782	48.9	814.7	17.0	0.0208	626.9
13	D	10.35	412.1	0.797	28.4	446.0	9.3	0.0208	628.3
14	D	9.93	886.2	1.261	96.6	1318.3	29.1	0.0221	627.6
15	D	9.93	412.1	1.199	42.7	546.8	14.0	0.0256	629.6
15	D	9.93	558.6	1.261	60.9	776.9	21.1	0.0272	628.9
16	L	14.08	611.8	1.388	73.4	792.6	15.8	0.0200	628.4
17	E	12.01	412.1	1.199	42.7	539.8	12.8	0.0237	629.6
17	E	12.01	558.6	1.261	60.9	754.7	18.9	0.0250	628.9
18	E	10.76	886.2	0.760	58.2	1003.8	21.7	0.0216	626.5
18	E	10.76	723.8	0.782	48.9	811.2	18.0	0.0222	626.9
18	E	10.76	412.1	0.797	28.4	441.7	9.7	0.0220	626.3
19	E	10.75	886.2	1.261	96.6	1306.9	29.1	0.0223	627.6
20	F	11.59	71.7	0.539	3.3	46.0	1.4	0.0308	630.4
21	F	12.42	412.1	1.199	42.7	543.9	13.2	0.0243	629.6
21	F	12.42	558.6	1.261	60.9	777.2	16.8	0.0216	628.9
22	F	11.59	71.7	0.873	5.4	49.7	1.4	0.0262	630.9
23	F	11.59	886.2	0.760	58.2	1022.5	22.0	0.0215	628.5
23	F	11.59	723.8	0.782	48.9	820.0	19.0	0.0232	626.9

FILM = Oxide prefilm (mg/dm sq). Negative values caused by measurement error

FLUX = (n/cm sq/sec) X 10

FLUENCE = (n/cm sq) x 10

TABLE 4 (Cont'd) (360°C)

SPEC	INGOT	FILM	DAYS	AVFLUX	FLUENCE	O-WTGN	H-WTGN	H/O	AVTEMP(K)
23	F	11.59	412.1	0.797	28.4	447.8	9.1	0.0203	628.3
24	F	10.76	886.2	1.261	96.6	1319.8	27.9	0.0211	627.8
25	F	0.41	71.7	0.873	5.4	54.2	1.1	0.0203	630.9
26	F	0.83	71.7	0.539	3.3	55.5	1.0	0.0180	630.4
27	G	12.83	886.2	0.760	58.2	953.4	20.1	0.0211	628.5
27	G	12.83	723.8	0.782	48.9	770.0	17.1	0.0222	628.9
27	G	12.83	412.1	0.797	28.4	418.5	8.2	0.0198	628.3
28	G	12.84	886.2	1.281	96.6	1241.3	31.5	0.0254	627.8
29	G	12.83	412.1	1.199	42.7	513.9	13.8	0.0269	629.8
29	G	12.83	558.6	1.281	60.9	736.0	23.3	0.0317	628.9
30	D	8.82	570.2	1.282	63.2	811.9	15.3	0.0188	628.2
31	D	11.41	570.2	0.218	10.7	432.6	9.5	0.0220	626.2
32	D	12.29	757.9	0.000	0.0	232.1	6.4	0.0276	627.2
33	E	11.41	570.2	1.282	63.2	793.7	15.9	0.0200	628.2
34	E	9.65	570.2	0.218	10.7	437.3	10.9	0.0249	628.2
35	E	11.41	757.9	0.000	0.0	245.3	5.7	0.0232	627.2
36	C	11.41	570.2	1.282	63.2	746.3	18.7	0.0251	628.2
37	N	1.86	723.8	0.000	0.0	283.1	4.8	0.0170	631.0
38	C	12.18	570.2	0.218	10.7	410.4	8.9	0.0217	628.2
39	N	1.86	829.6	0.000	0.0	261.6	4.1	0.0157	628.1
40	C	12.35	757.9	0.000	0.0	218.5	5.7	0.0261	627.2
41	N	2.07	1581.2	0.001	0.1	391.0	8.8	0.0226	618.1
42	N	1.86	481.5	0.055	2.3	345.5	4.3	0.0123	630.9
43	G	10.58	570.2	1.282	63.2	756.9	18.0	0.0238	628.2
44	G	11.46	570.2	0.218	10.7	426.7	10.9	0.0256	628.2
45	G	11.46	757.9	0.000	0.0	228.9	4.8	0.0210	627.2
46	B	12.35	570.2	1.282	63.2	804.3	18.4	0.0229	628.2
47	B	10.53	570.2	0.218	10.7	437.8	7.6	0.0174	626.2
48	B	11.47	757.9	0.000	0.0	240.4	4.7	0.0196	627.2
49	G	2.48	558.6	0.916	44.2	640.1	13.9	0.0217	628.3
50	G	2.06	481.5	1.002	41.7	581.4	12.6	0.0217	629.2
51	G	2.48	481.5	0.000	0.0	193.7	2.9	0.0150	629.6
51	G	2.48	829.6	0.000	0.0	271.0	5.6	0.0207	628.1
52	O	0.83	829.6	0.000	0.0	288.1	6.9	0.0205	627.2
53	O	14.08	886.2	0.315	24.1	779.7	14.8	0.0190	627.1
54	O	17.38	412.1	0.104	3.7	260.0	4.0	0.0155	627.9
55	O	13.06	829.6	0.000	0.0	269.8	7.6	0.0282	627.2
56	O	13.06	71.7	0.000	0.0	15.2	0.3	0.0196	632.6
57	O	14.49	71.7	0.175	1.1	38.6	0.5	0.0130	629.8
58	O	14.90	412.1	1.147	40.8	550.4	13.4	0.0243	629.7
58	O	14.90	886.2	1.210	92.6	1284.2	25.6	0.0199	628.0
58	O	14.90	558.6	1.215	58.6	798.0	17.9	0.0224	629.1
59	O	14.08	412.1	0.000	0.0	103.1	2.0	0.0194	630.0
60	O	14.91	71.7	0.851	5.3	54.4	1.4	0.0257	630.9
61	P	1.86	829.6	0.000	0.0	267.6	6.2	0.0232	628.1
62	Q	0.00	829.6	0.000	0.0	268.1	5.7	0.0213	627.9
63	Q	-2.48	558.6	0.000	0.0	237.2	3.7	0.0156	631.4
64	Q	0.41	723.8	0.000	0.0	326.8	4.1	0.0125	630.6
65	Q	1.24	558.6	1.000	48.3	763.5	18.3	0.0240	629.4

TABLE 4 (Cont'd) (360°C)

SPEC	INGOT	FILM	DAYS	AVFLUX	FLUENCE	O-WTGN	H-WTGN	H/O	AVTEMP(K)
66	Q	0.83	481.5	0.937	39.0	652.3	12.0	0.0185	630.6
67	Q	0.83	558.6	0.000	0.0	177.9	3.6	0.0202	629.6
68	Q	2.07	481.5	0.000	0.0	153.6	3.4	0.0223	629.5
69	Q	2.49	417.5	0.000	0.0	89.9	0.5	0.0056	625.8
70	B	2.06	474.1	1.110	45.5	480.6	8.9	0.0185	625.5
71	B	2.48	311.7	0.000	0.0	121.3	0.7	0.0058	628.9
71	B	2.48	547.2	0.000	0.0	159.2	1.9	0.0121	628.9
72	B	2.48	474.1	1.180	48.3	486.8	10.3	0.0212	625.5
73	I	12.34	317.4	0.163	4.5	190.9	4.8	0.0249	624.0
74	I	11.84	317.4	0.020	0.5	159.1	0.0	0.0003	628.4
75	H	12.60	317.4	0.163	4.5	187.8	5.8	0.0307	624.0
76	H	13.73	317.4	0.020	0.5	154.8	0.8	0.0050	628.4
77	B	12.16	317.4	0.163	4.5	183.5	4.5	0.0244	624.0
78	B	13.20	317.4	0.020	0.5	165.4	2.2	0.0135	628.4
79	V	15.36	317.4	0.020	0.5	134.1	1.9	0.0139	628.4
80	V	14.71	317.4	0.163	4.5	181.6	4.7	0.0261	624.0
81	B	0.82	400.7	0.001	0.0	145.1	2.2	0.0151	628.5
82	A	10.65	71.7	0.539	3.3	51.8	0.6	0.0116	630.4
83	A	11.44	886.2	0.760	58.2	1039.4	14.6	0.0140	626.5
83	A	11.44	723.8	0.782	48.9	837.2	15.4	0.0184	626.9
83	A	11.44	412.1	0.797	28.4	455.2	7.7	0.0169	628.3
84	A	11.46	71.7	0.873	5.4	57.1	1.0	0.0175	630.9
85	A	11.47	886.2	1.261	96.6	1276.3	24.1	0.0189	627.6
86	A	9.55	412.1	1.199	42.7	553.3	10.4	0.0186	629.6
86	A	9.55	558.6	1.261	60.9	776.2	15.5	0.0200	628.9
87	A	0.41	71.7	0.539	3.3	57.2	0.9	0.0157	630.4
88	A	-1.06	71.7	0.873	5.4	52.9	0.7	0.0132	630.9

310°C (530°F)

SPEC	INGOT	FILM	DAYS	AVFLUX	FLUENCE	O-WTGN	H-WTGN	H/O	AVTEMP(K)
89	B	12.00	1569.9	0.000	0.0	41.3	1.6	0.0378	580.1
90	B	10.25	997.5	1.471	126.7	208.2	7.2	0.0346	584.4
91	F	11.10	1210.3	1.471	153.8	943.8	11.5	0.0122	584.1
92	U	16.17	804.2	1.489	103.5	163.3	1.9	0.0116	582.1
93	D	8.77	997.5	1.661	143.1	337.7	4.0	0.0118	586.1
94	D	11.41	907.7	0.594	46.6	213.5	4.7	0.0220	588.4
94	D	11.41	1464.3	0.609	77.0	513.8	10.2	0.0199	588.2
95	E	9.66	997.5	1.661	143.1	326.5	5.5	0.0168	586.1
96	E	10.44	907.7	0.594	46.6	192.3	4.6	0.0239	588.4
96	E	10.44	1464.3	0.609	77.0	480.8	10.5	0.0216	588.2
97	C	11.41	997.5	1.661	143.1	229.3	5.3	0.0231	586.1
98	C	11.41	907.7	0.594	46.6	153.8	1.9	0.0124	588.4
99	C	11.41	1464.3	0.609	77.0	411.0	8.7	0.0212	588.2
100	G	9.70	897.5	1.661	143.1	509.9	5.9	0.0116	586.1

TABLE 4 (Cont'd) (310°C)

SPEC	INGOT	FILM	DAYS	AVFLUX	FLUENCE	O-WTGN	H-WTGN	H/O	AVTEMP(K)
101	G	10.59	907.7	0.594	46.8	175.0	3.9	0.0223	588.4
101	G	10.59	1464.3	0.609	77.0	568.9	6.6	0.0116	588.2
102	B	12.35	997.5	1.661	143.1	319.5	5.8	0.0182	588.1
103	B	11.46	907.7	0.594	46.8	217.2	5.0	0.0230	588.4
103	B	11.46	1464.3	0.609	77.0	502.8	9.9	0.0198	588.2
103	B	11.46	2107.8	0.623	113.4	961.1	19.5	0.0202	588.0
104	I	11.70	838.2	1.697	122.9	98.3	3.6	0.0365	584.8
104	I	11.70	999.8	1.713	148.0	283.0	4.4	0.0155	584.2
105	I	12.37	999.8	0.300	25.9	103.5	3.8	0.0368	580.1
105	I	12.37	838.2	0.304	22.0	76.1	2.8	0.0368	580.7
106	H	13.18	999.8	1.713	148.0	396.6	8.6	0.0218	584.2
107	H	12.91	999.8	0.300	25.9	106.0	3.7	0.0347	580.1
107	H	12.91	838.2	0.304	22.0	75.4	2.4	0.0325	580.7
108	J	12.81	999.8	1.713	148.0	470.2	5.7	0.0122	584.2
109	J	14.49	999.8	0.300	25.9	95.3	4.2	0.0445	580.1
109	J	14.49	838.2	0.304	22.0	68.4	2.1	0.0304	580.7
110	B	11.73	838.2	1.697	122.9	108.6	3.2	0.0292	584.8
110	B	11.73	999.8	1.713	148.0	237.4	5.9	0.0249	584.2
111	V	13.96	838.2	1.697	122.9	162.8	3.5	0.0218	584.7
111	V	13.96	999.8	1.713	148.0	480.2	8.3	0.0173	584.2
112	V	15.01	999.8	0.300	25.9	116.3	3.3	0.0281	580.1
112	V	15.01	838.2	0.304	22.0	84.5	4.6	0.0539	580.7
113	B	2.05	1406.5	1.388	168.7	744.7	14.7	0.0198	586.2
114	S	13.67	804.2	1.489	103.5	113.0	1.5	0.0130	582.1
115	W	10.00	543.3	0.000	0.0	12.4	0.1	0.0121	588.4
116	W	10.80	543.3	1.355	63.6	57.4	1.1	0.0183	588.7
117	W	10.40	155.3	1.340	18.0	13.0	0.7	0.0522	586.7
118	W	10.80	155.3	1.340	18.0	13.9	0.2	0.0151	586.7
119	W	10.00	387.9	1.340	44.9	28.1	0.6	0.0208	588.2
120	B	8.90	538.0	0.528	24.5	37.2	0.8	0.0212	584.4
121	B	9.92	1745.4	1.196	180.4	1051.5	18.4	0.0156	587.3
121	B	9.92	2048.0	1.198	212.0	1421.6	20.0	0.0141	587.2
122	B	9.80	538.0	1.271	59.1	32.7	0.5	0.0153	587.2
123	A	1.46	2045.7	0.465	82.2	722.2	9.6	0.0132	588.2
124	A	9.75	1297.3	1.537	172.3	394.2	5.4	0.0137	584.9
124	A	9.75	2045.7	1.585	280.1	1215.5	17.0	0.0140	584.6
125	A	9.75	1297.3	0.437	49.0	336.2	5.6	0.0167	588.3
125	A	9.75	2045.7	0.465	82.2	727.1	11.1	0.0152	588.2
126	F	10.57	1297.3	0.437	49.0	351.1	11.3	0.0322	588.3
126	F	10.57	2045.7	0.465	82.2	848.5	24.6	0.0290	588.2
127	F	9.76	1297.3	1.537	172.3	923.0	15.6	0.0169	584.9
127	F	9.76	2045.7	1.585	280.1	2279.8	30.8	0.0135	584.6
128	F	0.98	2045.7	0.465	82.2	811.3	21.5	0.0265	588.2
129	B	0.65	1297.3	1.537	172.3	665.4	9.3	0.0140	584.9
130	B	0.74	1297.3	0.437	49.0	352.8	5.4	0.0153	588.3
130	B	0.74	2045.7	0.465	82.2	776.7	14.0	0.0180	588.2
131	D	8.94	1297.3	1.537	172.3	631.7	12.9	0.0204	584.9
131	D	8.94	2045.7	1.585	280.1	1927.3	24.7	0.0128	584.8
132	D	8.94	1297.3	0.437	49.0	337.1	7.1	0.0211	588.3

TABLE 4 (Cont'd) (310°C)

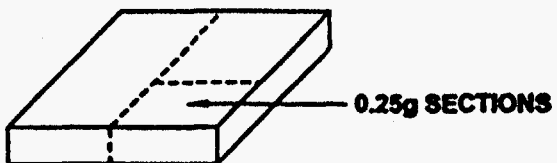
SPEC	INGOT	FILM	DAYS	AVFLUX	FLUENCE	O-WTGN	H-WTGN	H/O	AVTEMP(K)
132	D	8.94	2045.7	0.465	82.2	793.9	15.0	0.0189	588.2
133	D	0.81	2045.7	0.465	82.2	785.2	15.3	0.0195	588.2
134	E	8.95	1297.3	1.537	172.3	568.3	7.5	0.0132	584.9
135	E	8.94	1297.3	0.437	49.0	338.0	6.7	0.0198	588.3
135	E	8.94	2045.7	0.465	82.2	823.4	17.2	0.0209	588.2
136	C	8.94	2045.7	1.585	280.1	1479.2	22.4	0.0151	584.6
137	C	0.98	1297.3	1.537	172.3	461.1	9.5	0.0208	584.9
138	C	0.98	1297.3	0.437	49.0	287.0	6.1	0.0213	588.3
138	C	0.98	2045.7	0.465	82.2	669.0	14.6	0.0218	588.2
139	G	8.95	1297.3	1.537	172.3	958.9	10.4	0.0108	584.9
140	G	8.94	1297.3	0.437	49.0	329.8	7.8	0.0230	588.3
140	G	8.94	2045.7	0.465	82.2	910.4	17.3	0.0190	588.2

TABLE 5 - Chemistry of the Zircaloy-4* Exposed in the Advanced Test Reactor
(ppm by weight)

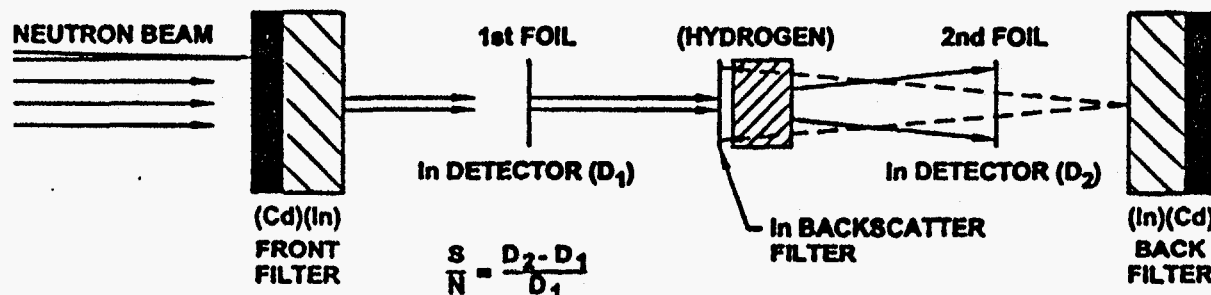
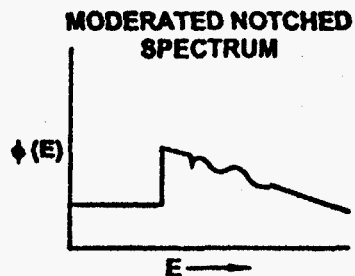
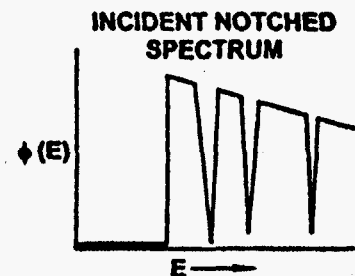
INGOT	MELTS	Sn	Fe	O	Cr	Al	C	Cu	Hf	Mn	Ni	Nb	Si	Ta	Ti
A	2	14400	1500	780	80	35	101	<40	<125	<25	15	<100	55	<200	<5
B	2	14300	2100	1400	1140	<35	<135	<25	83	<25	<35	<50	<60	<100	<5
C	2	13200	2300	1400	1100	<35	<135	<25	<80	<25	<35	<50	<60	<100	<5
D	2	14500	1800	1400	1200	<35	<135	28	82	<25	<35	<50	<60	<100	<5
E	2	14800	2000	1300	1100	<35	<135	<25	88	<25	<35	<50	<60	<100	<5
F	2	13700	2100	1255	1000	30	180	<10	73	<10	-	<100	<40	<200	15
G	2	14800	2000	980	1000	<35	30	14	58	<25	<35	-	50	-	<5
H	2	16800	2100	1200	1100	45	148	38	81	<25	<35	<50	74	<100	<5
I	2	15100	2100	1400	1000	45	<100	32	84	<25	<35	<50	75	<100	<5
J	3	14400	2100	1300	1000	40	<100	27	<80	<25	<35	<50	71	<100	<5
L	2	15500	2100	1400	1100	44	108	<25	<80	<25	<35	<50	80	<100	<5
M	2	15400	2100	1028	1000	42	108	<25	<80	<25	<35	<50	82	<100	<5
N	2	16000	2100	1400	1000	42	110	<25	<80	<25	<35	<50	85	<100	<5
O	2	16200	2100	1400	1100	48	130	<25	<80	<25	<35	<50	78	<100	<5
P	2	15500	2100	1400	1100	43	133	<25	<80	<25	<35	<50	82	<100	<5
Q	2	15300	2100	1400	1100	45	133	<25	<80	<25	<35	<50	87	<100	<5
R	3	15800	1810	1400	1100	58	80	27	88	7	28	20	18	8	15
S	3	15900	1810	1400	1100	58	80	27	88	7	28	20	18	8	15
T	3	15800	2320	1400	1100	48	180	10	41	6	28	19	130	12	12
U	3	15800	2320	1400	1100	48	180	10	41	6	28	19	130	12	12
V	3	14400	2200	1300	1000	50	<100	<25	<80	<25	<35	<50	88	<100	<5
W	3	15100	2100	1200	900	28	123	18	42	<10	17	-	42	<100	<5

*The "A" parameter $A = \sum t_i / \text{loop} (-79480/RT)$ where t_i and T_i are post beta quench anneal times and temperatures for the alpha annealed coupons produced from these Ingots is $A = 2.7 \times 10^{16}$.

I. INERT GAS FUSION OF CORROSION COUPON SECTIONS



II. NEUTRON BEAM ATTENUATION



EXPERIMENTAL ARRANGEMENT FOR NOTCHED
SPECTRUM MEASUREMENTS

Figure 1 Methods Use to Measure the Hydrogen Pickup

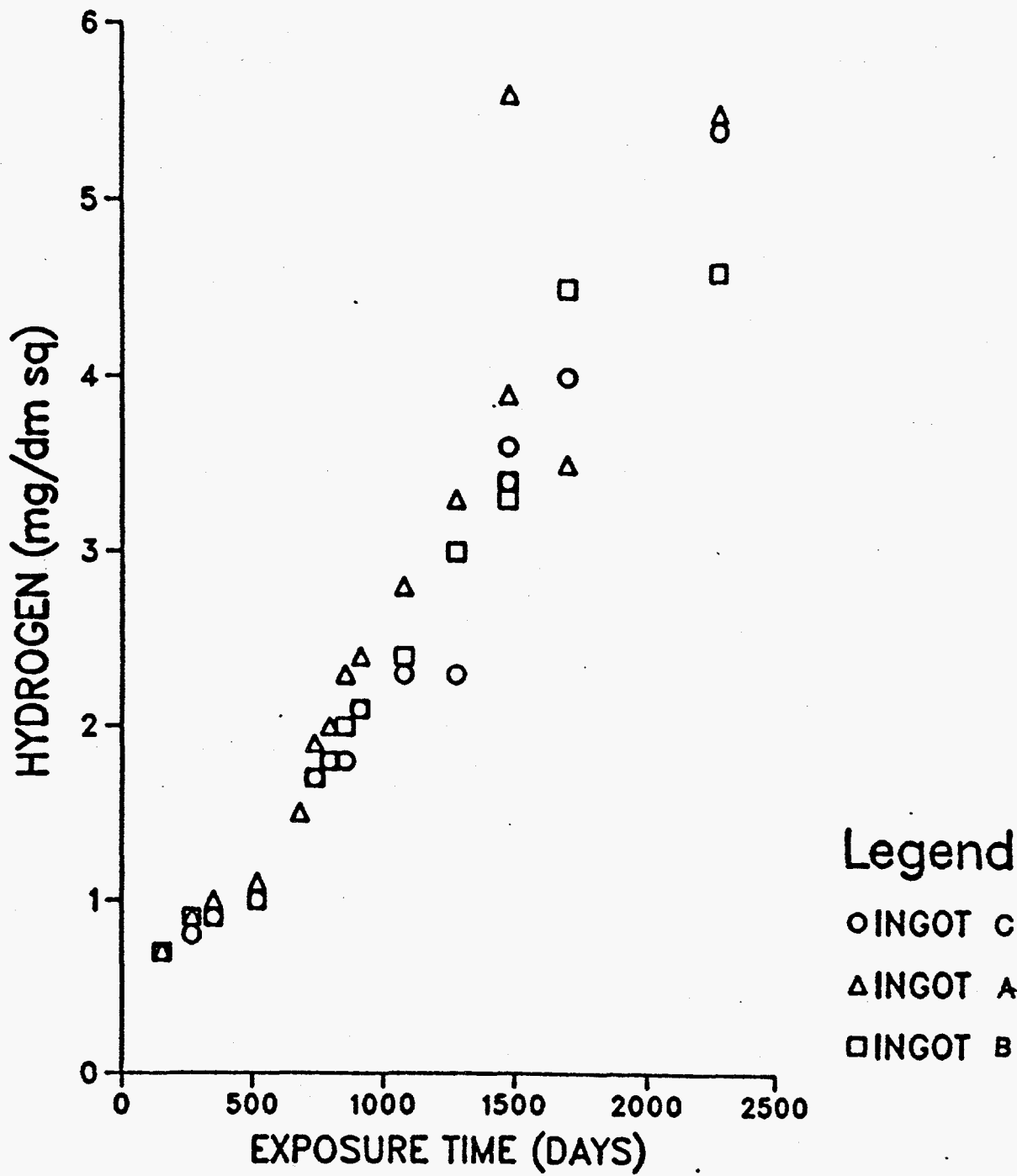


Figure 2 Hydrogen Pickup of Alpha-Annealed Zircaloy-4 Exposed in Autoclave at 316°C

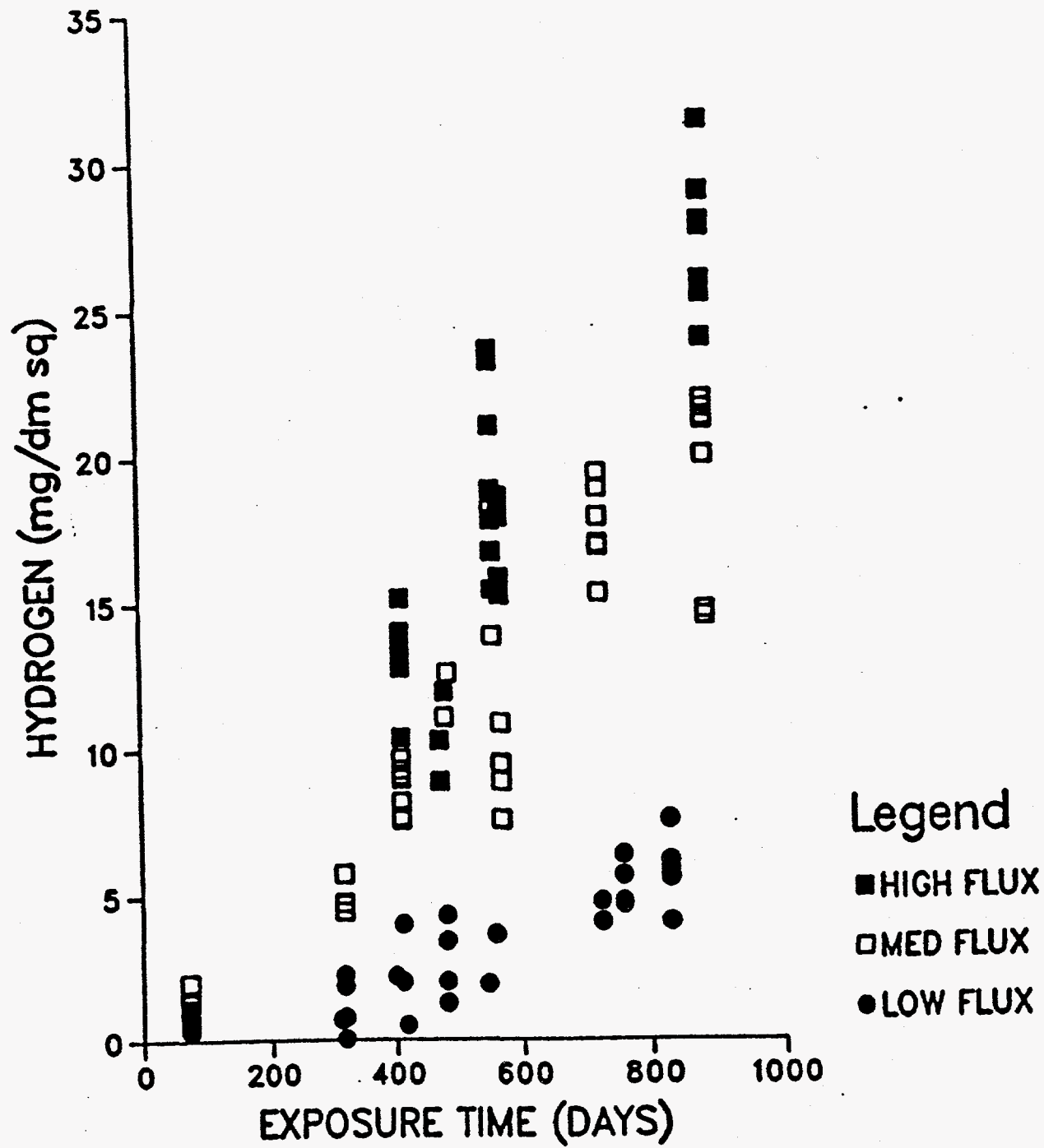


Figure 3 Hydrogen Pickup of Alpha-Annealed Zircaloy-4 Exposed in the ATR at 360°C

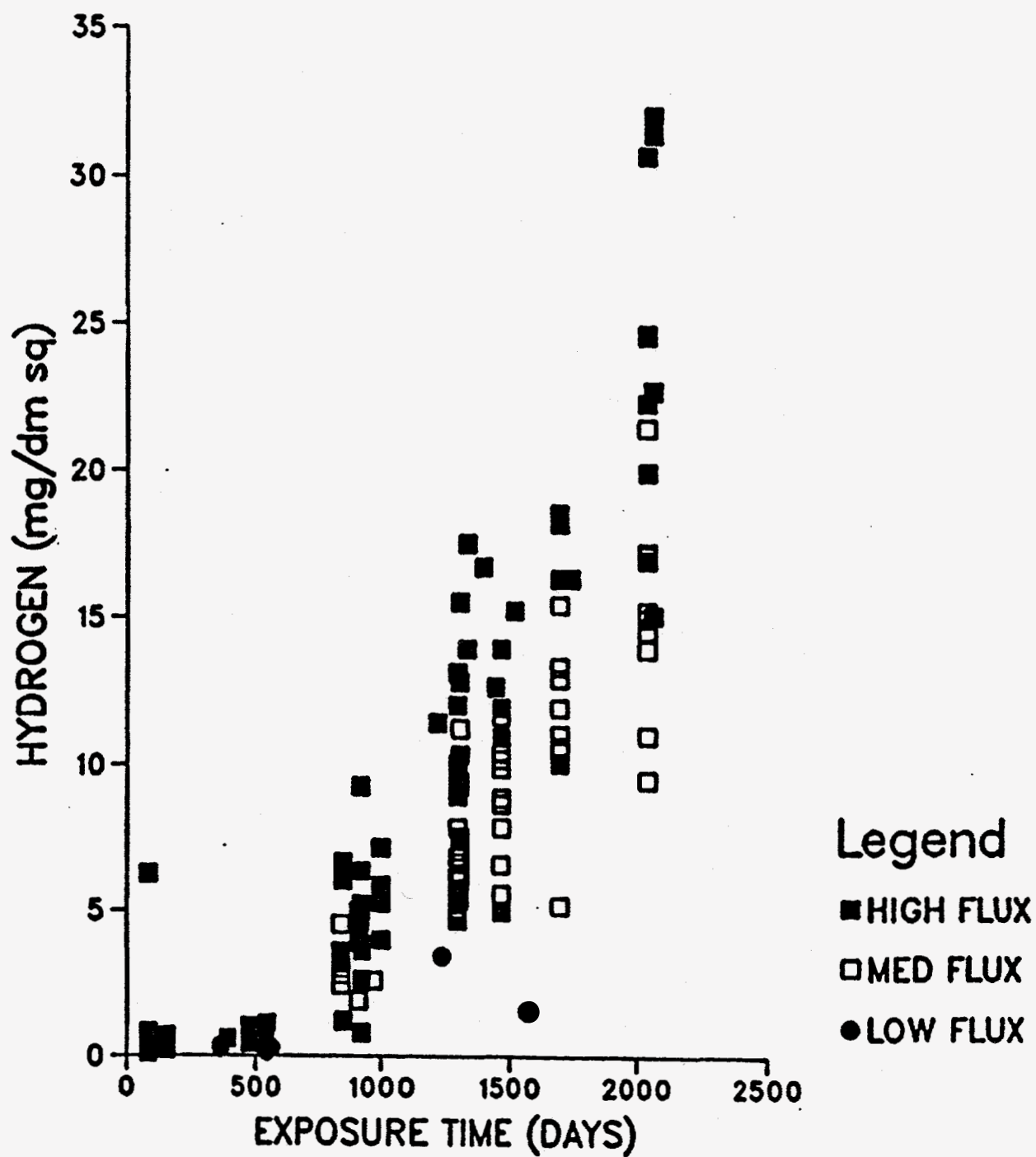


Figure 4 Hydrogen Pickup of Alpha-Annealed Zircaloy-4 Exposed in the ATR at 310°C

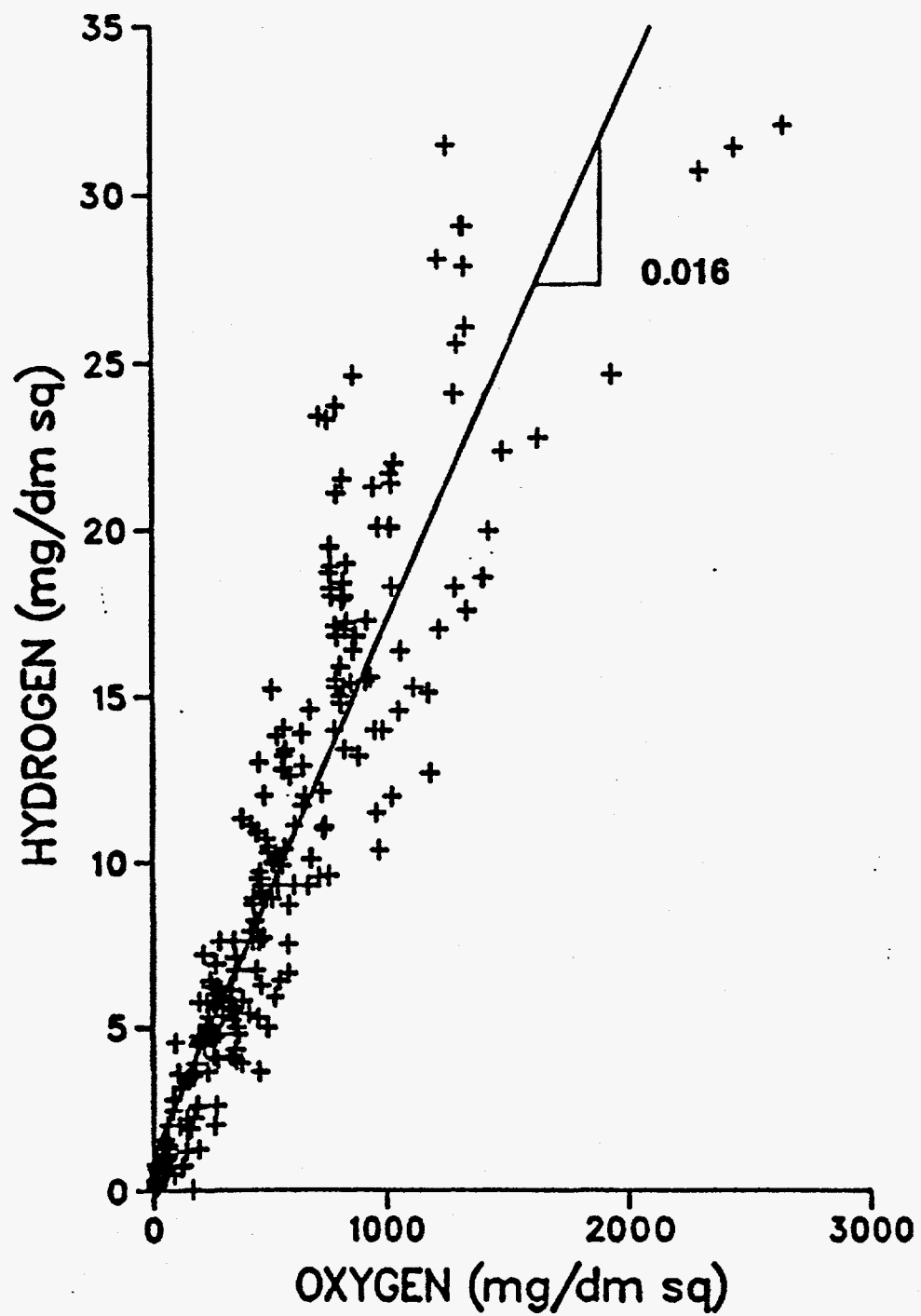


Figure 5 Hydrogen Pickup of Alpha-Annealed Zircaloy-4 Exposed in the ATR at 310 and 360°C Versus Oxygen Weight Gain

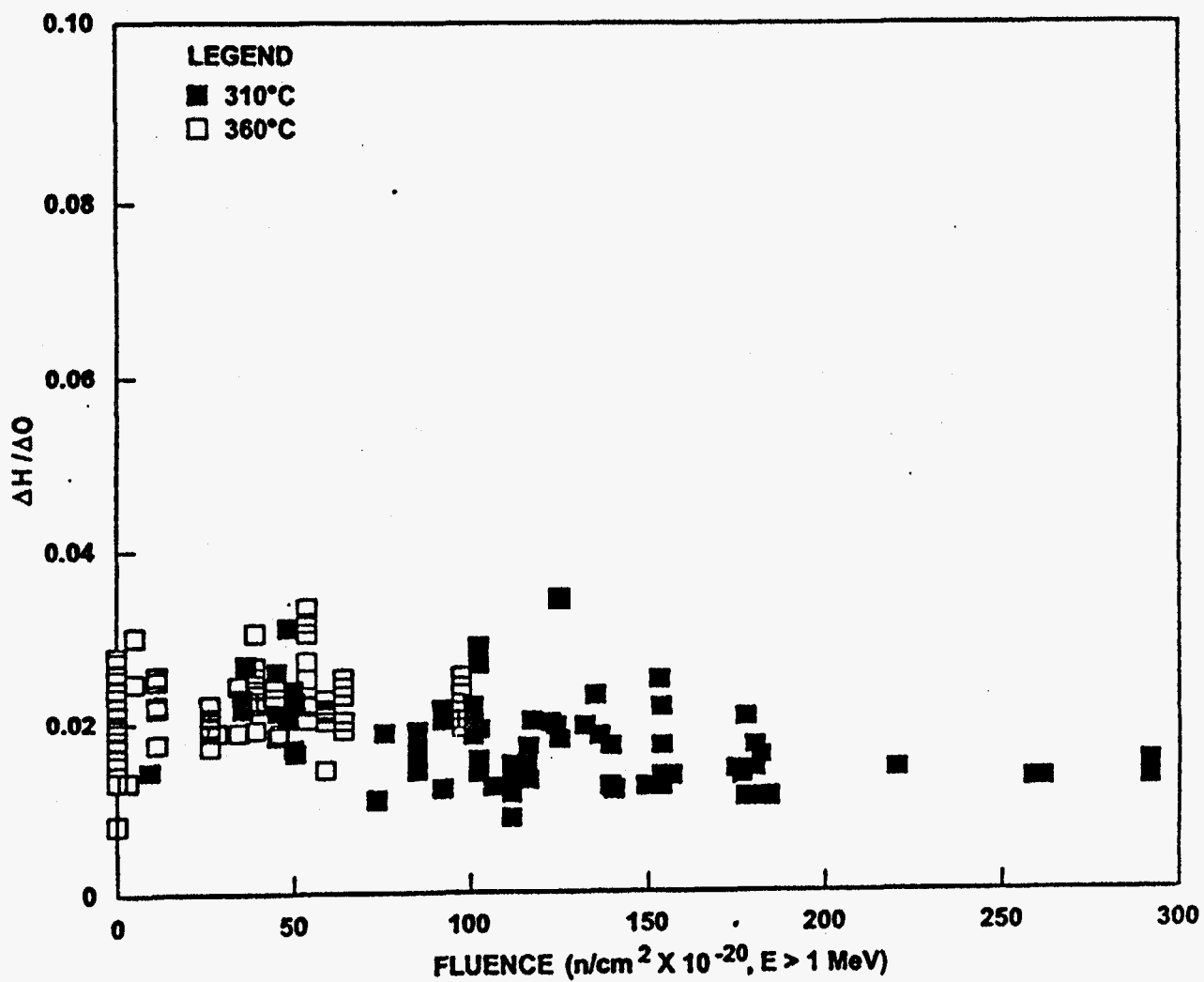
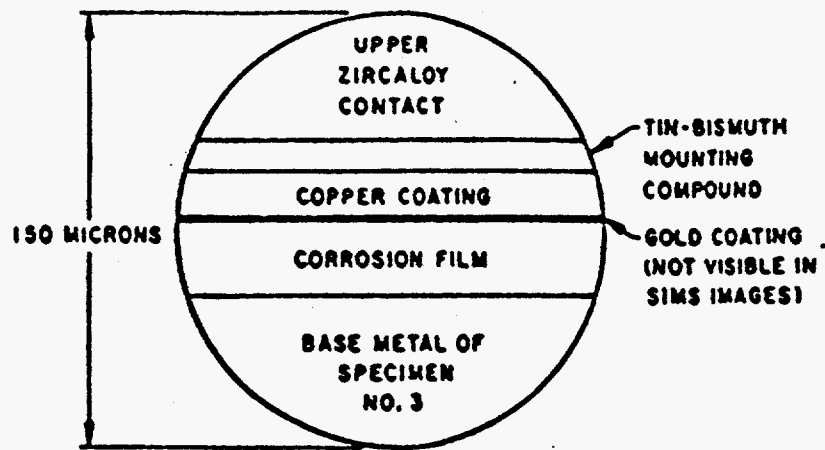


Figure 6 Hydrogen-to-Oxygen Weight Gain Ratio of Alpha-Annealed Zircaloy-4 Exposed in the ATR Versus Fluence

360°C WATER FILM

FILM THICKNESS $25\mu\text{m}$

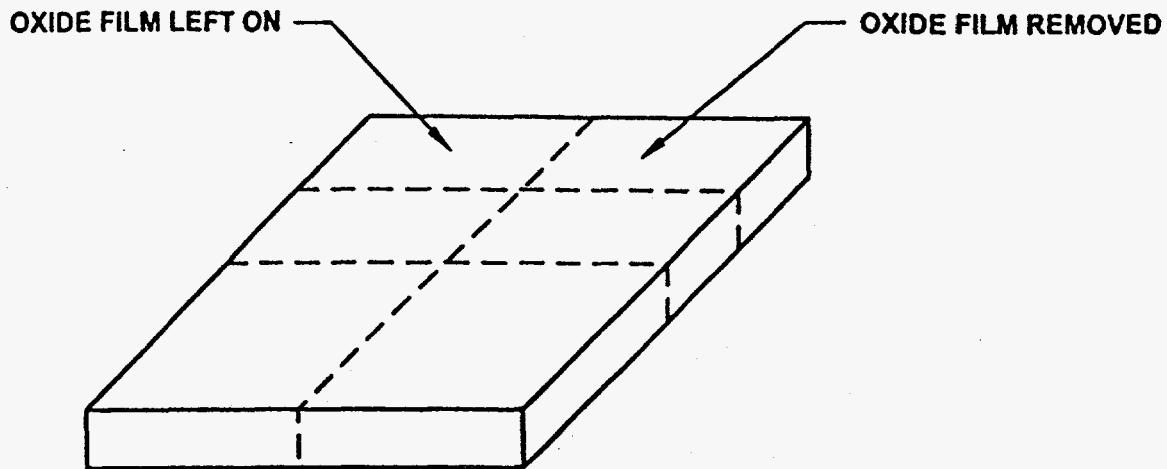
TRANSVERSE SECTION OF SPECIMEN AS SEEN
IN A $150\mu\text{m}$ FIELD SIMS IMAGE



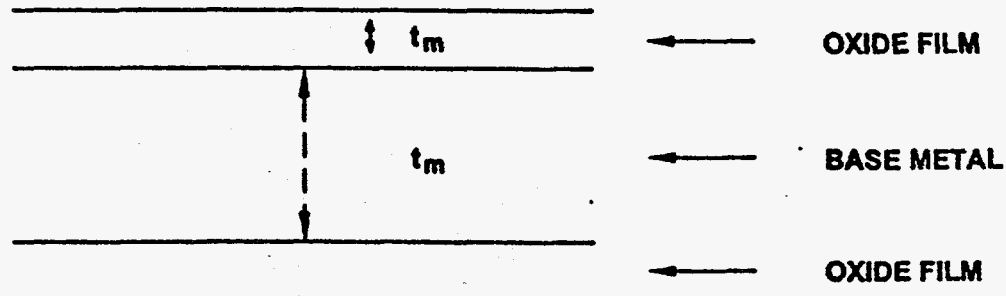
^1H SIMS IMAGE OF A SECOND PORTION OF SPECIMEN #3.
Cs PRIMARY BEAM, 150 MICRON FIELD, 60 SECOND DATA COLLECTION.

Figure 7 Hydrogen Distribution in the Oxide Film and Metal Substrate

INERT GAS FUSION⁺ OF SAMPLES WITH AND WITHOUT OXIDE FILMS



CONCENTRATION OF OXIDE FILM FOUND AS FOLLOWS



$$C_T (t_m \rho_m + 2t_o \rho_o) = C_m t_m \rho_m + 2C_o t_o \rho_o \quad (1)$$

WHERE C_T - IS THE TOTAL HYDROGEN CONCENTRATION OF THE SAMPLE MEASURED WITH THE OXIDE FILM LEFT ON (PPM BY WEIGHT)

C_m - IS THE HYDROGEN CONCENTRATION OF THE METAL (PPM BY WEIGHT)

C_o - IS THE HYDROGEN CONCENTRATION OF THE OXIDE (PPM BY WEIGHT)

t_m - IS THE BASE METAL THICKNESS (CM)

t_o - IS THE OXIDE FILM THICKNESS (CM)

ρ_m - IS THE DENSITY OF ZIRCALOY (6.545 G/CM³)

ρ_o - IS THE DENSITY OF THE OXIDE FILM (5.65 G/CM³)

+ SAMPLE MELTED AND VOLUME OF HYDROGEN RELEASED DETERMINED.

Figure 8 Method Used to Determine Hydrogen in the Oxide Film

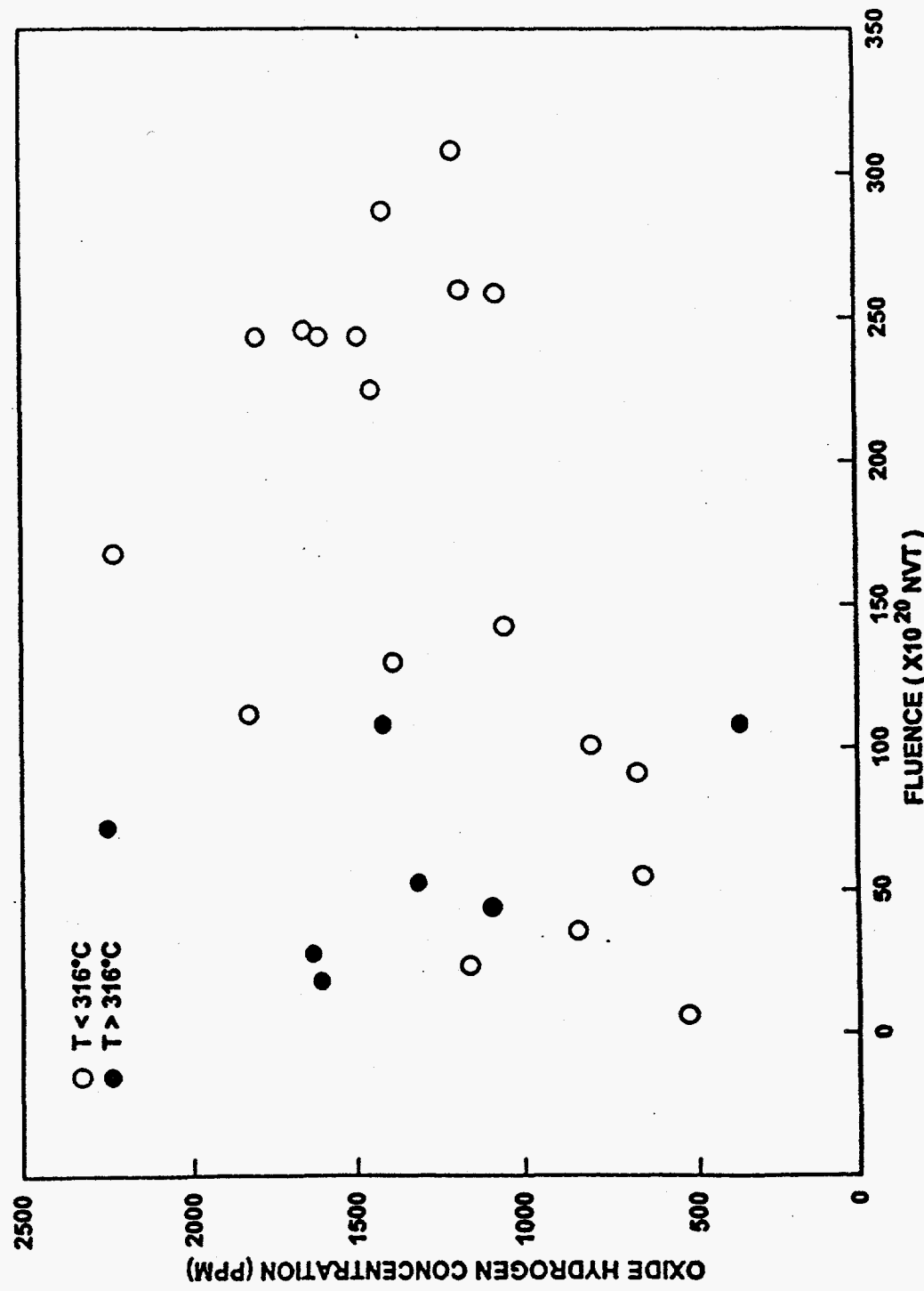
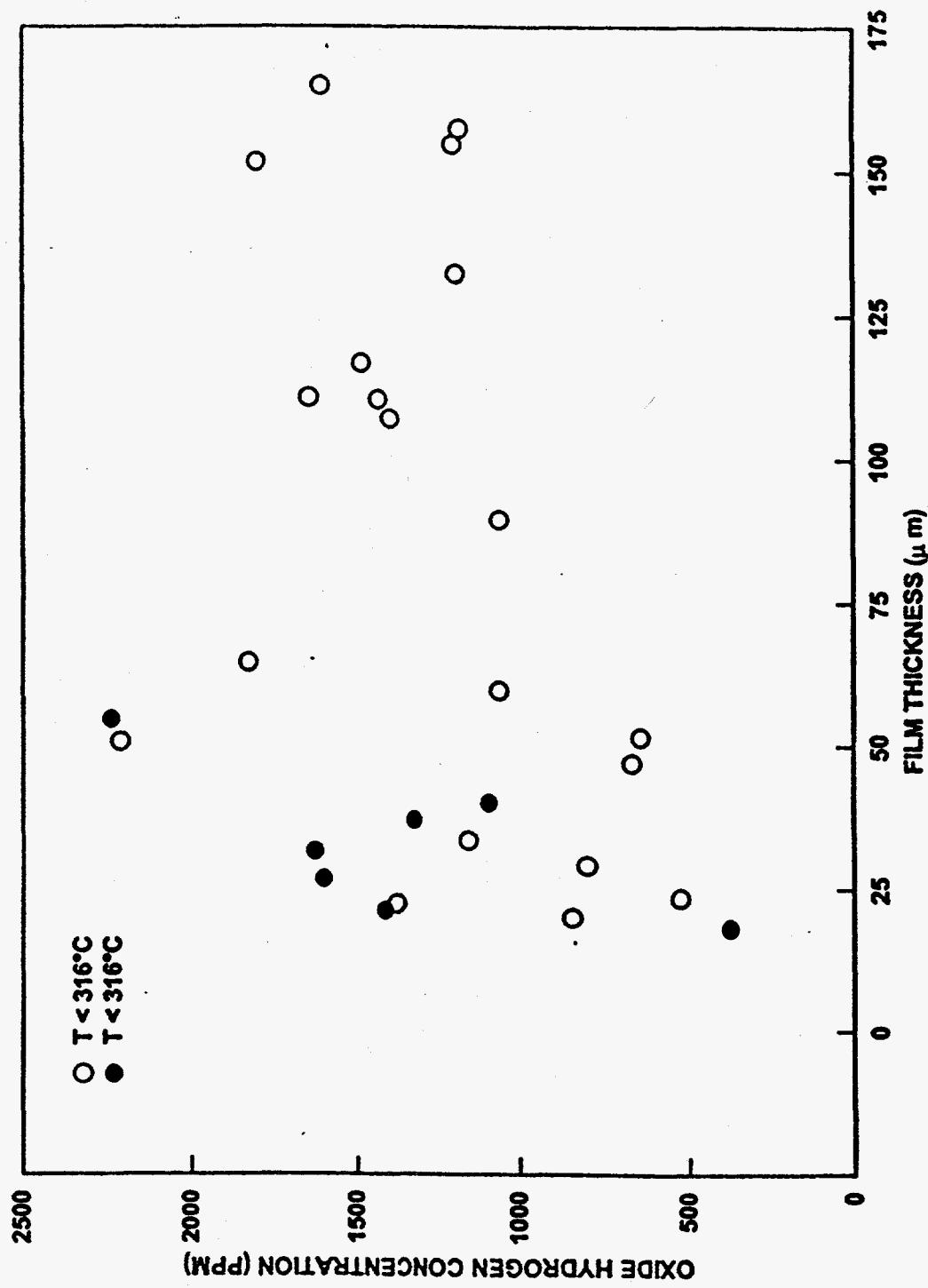


Figure 9 Hydrogen Concentration In the Oxide Film as a Function of Fluence



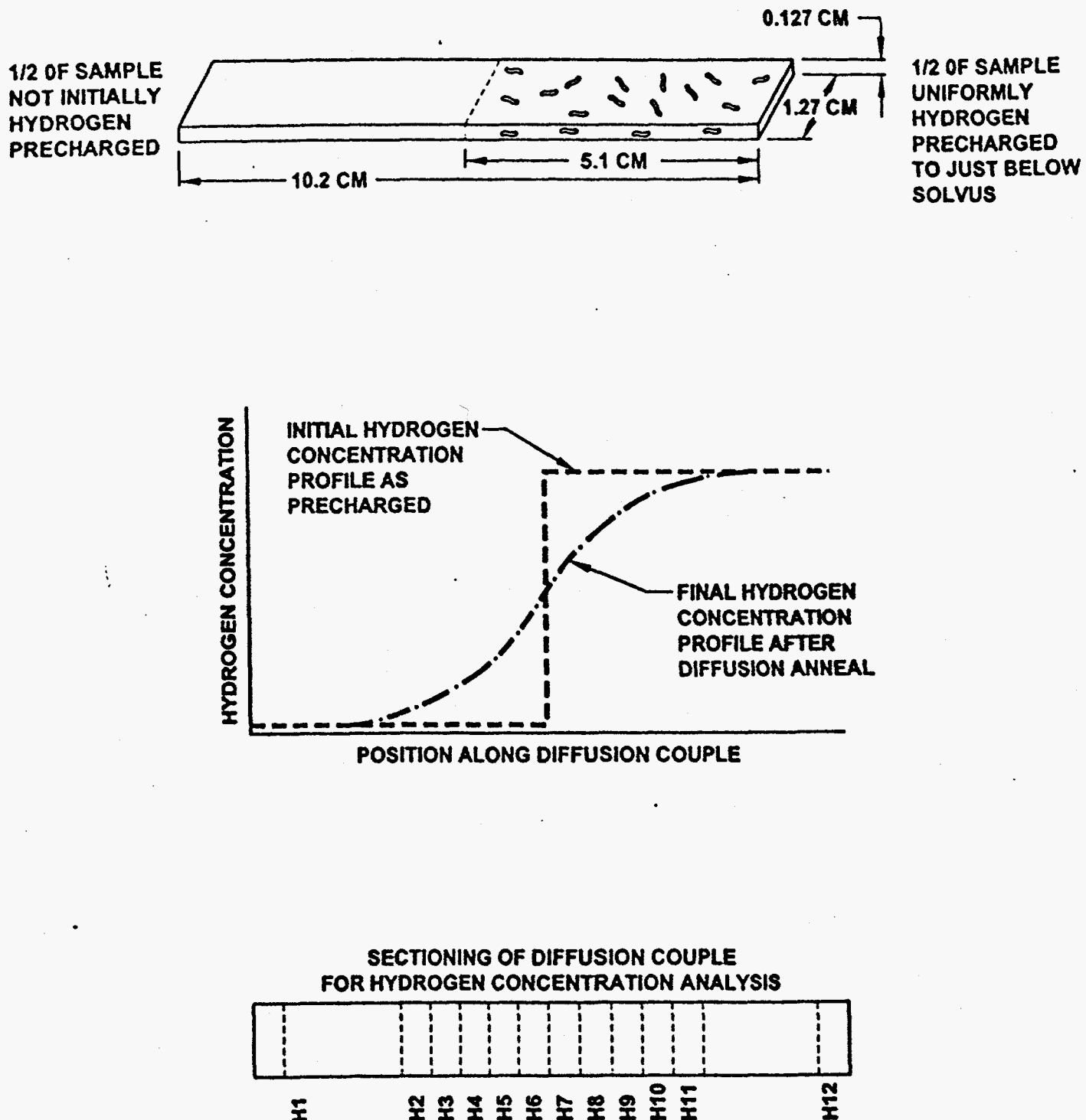


Figure 11 Preparation and Testing Sequence of Samples to Determine the Hydrogen-Diffusion Kinetics and Hydrogen Solvus

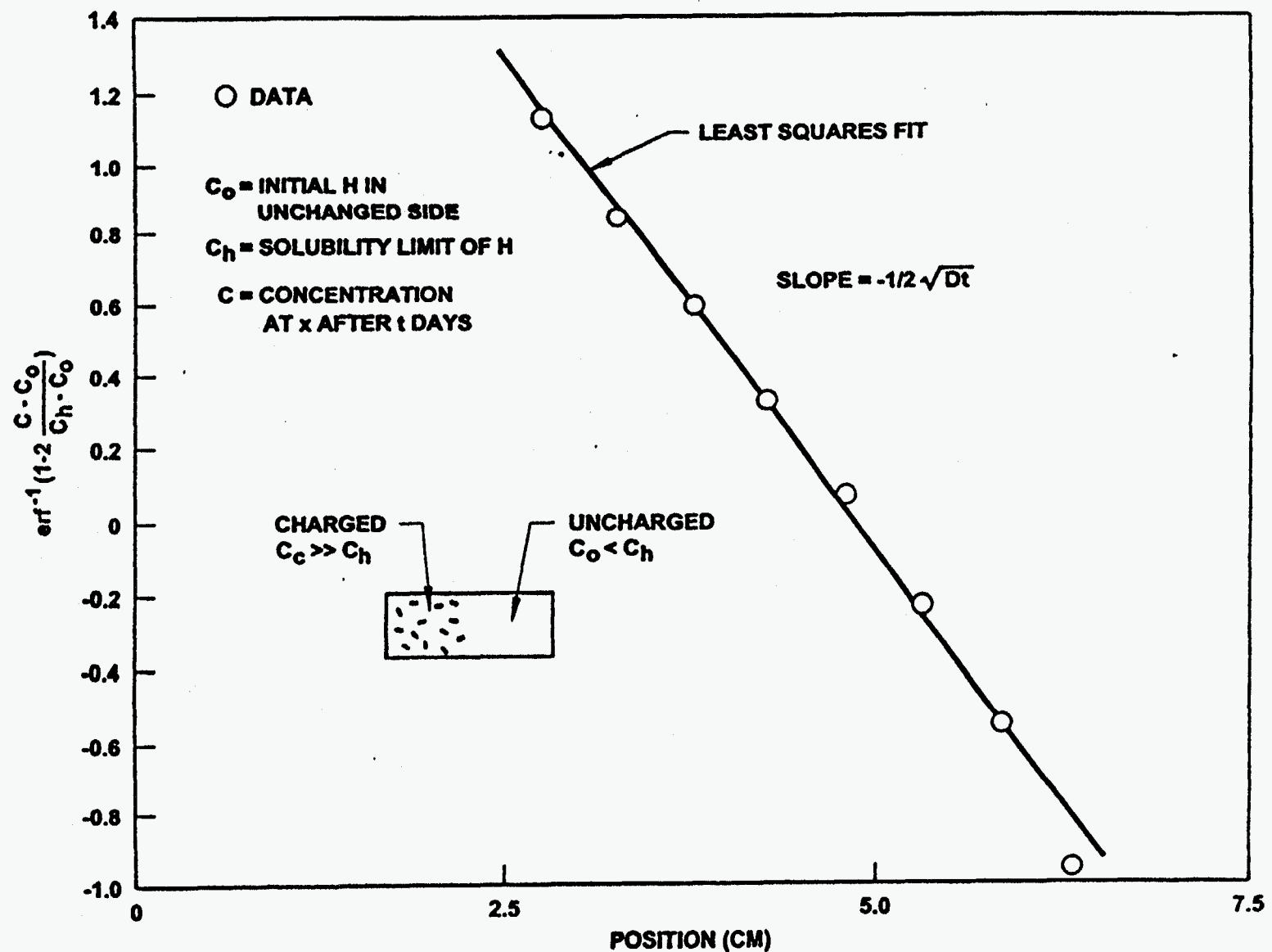


Figure 12 Alpha-Annealed Zircaloy-4 Diffusion Couple Results After Exposure of 3.9 Days at 427°C

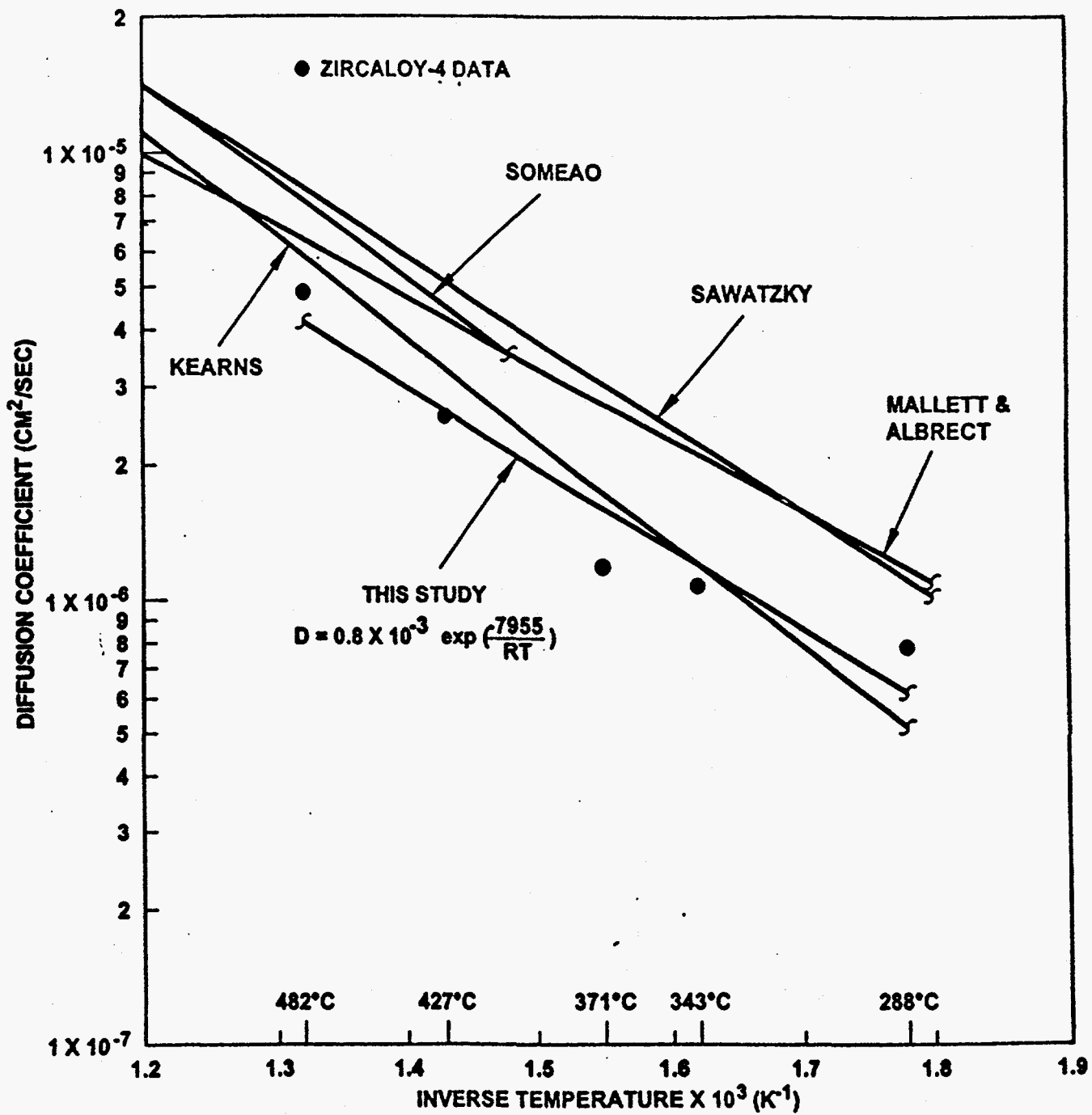


Figure 13 Diffusion Coefficient of Hydrogen In Alpha-Zirconium as a Function of Temperature

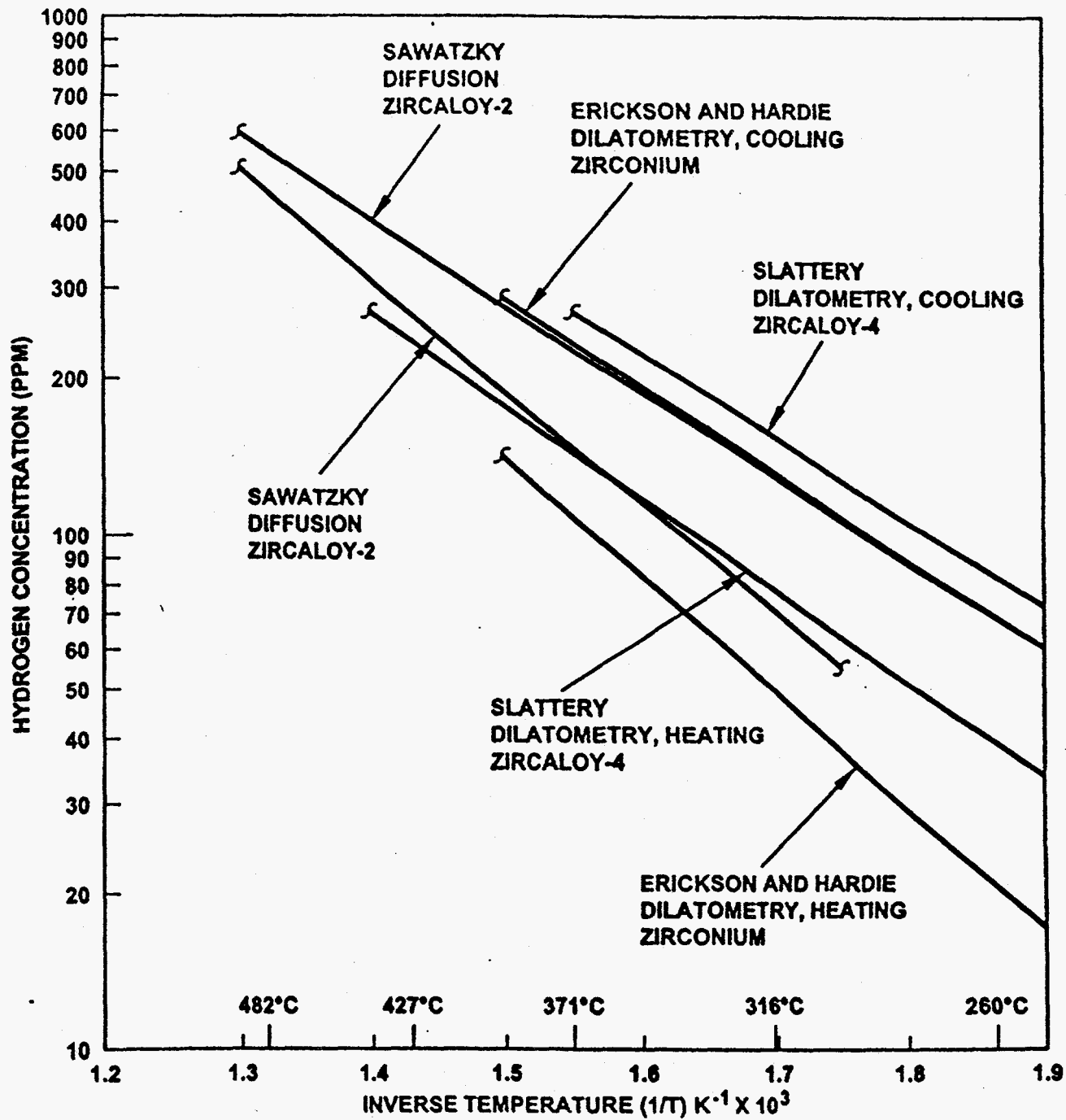
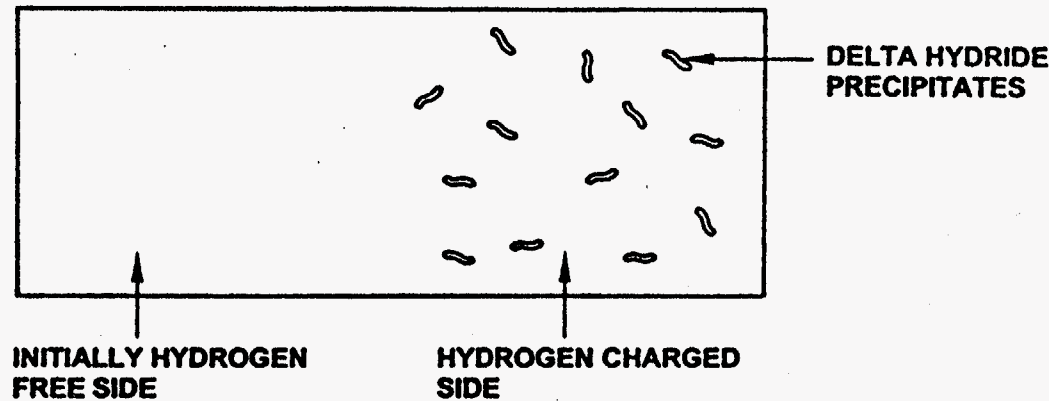
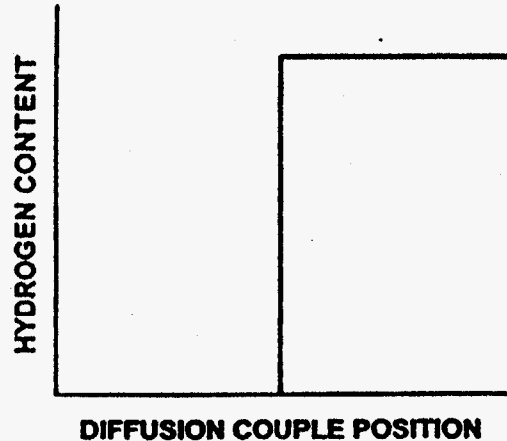


Figure 14 Hydrogen Solvus in Zirconium Alloys as a Function of Temperature

TEMPERATURE UNIFORM ACROSS SAMPLE



PREANNEAL



POSTANNEAL

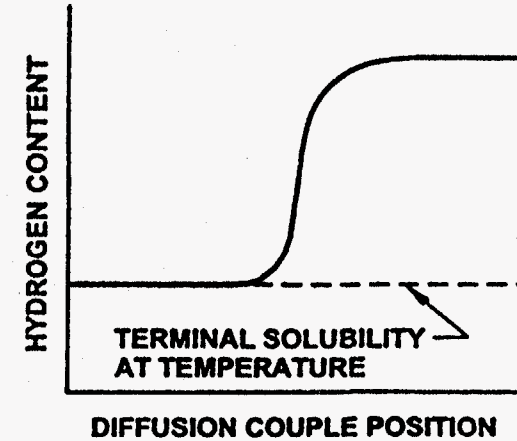


Figure 15 Determination of the Solvus on Dissolution by the Diffusion Method

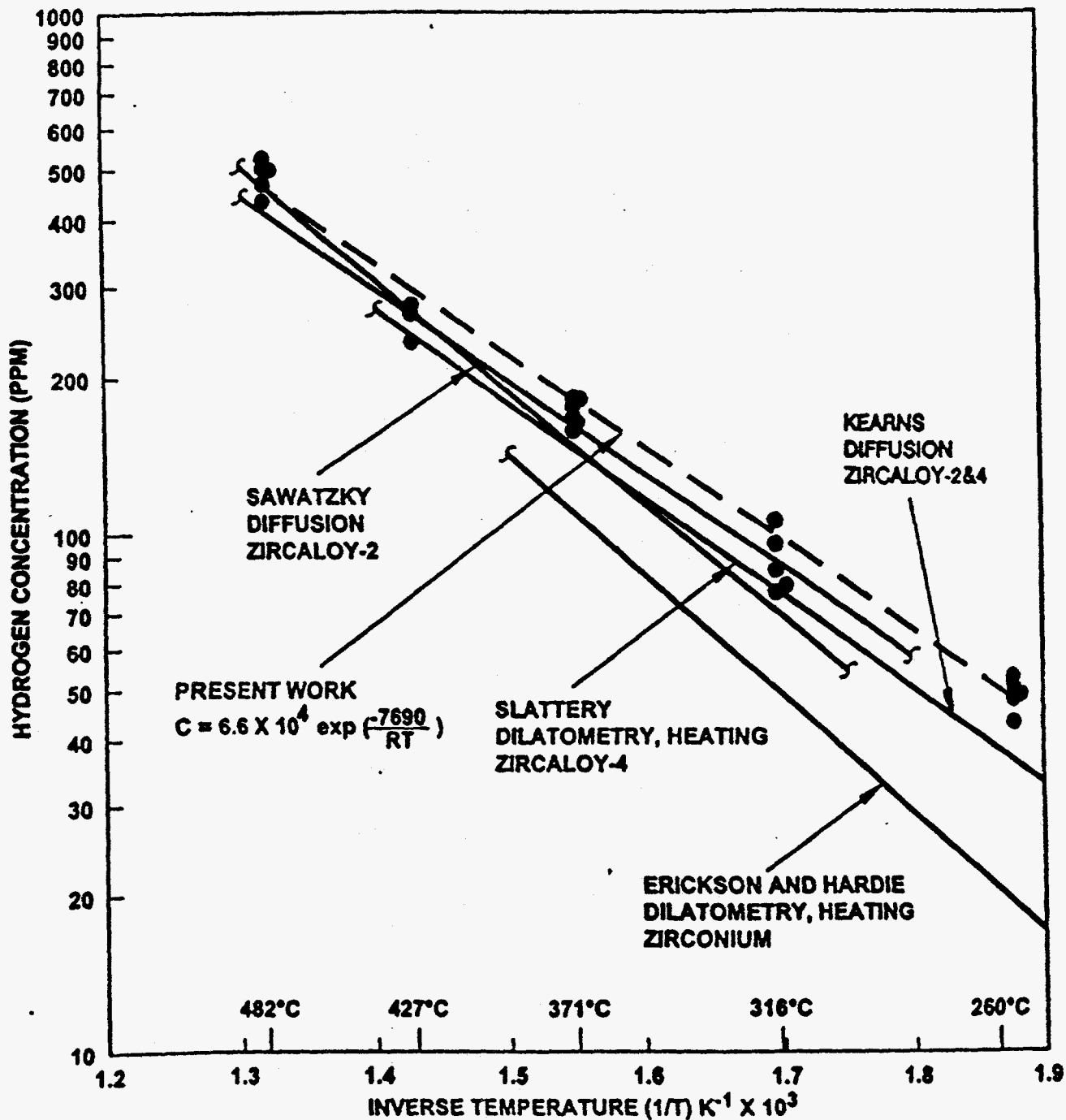
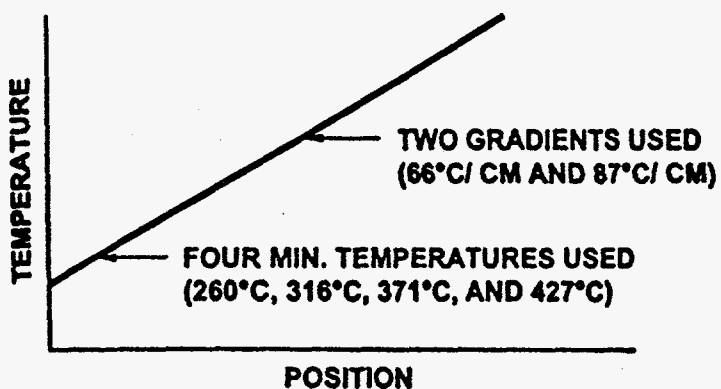
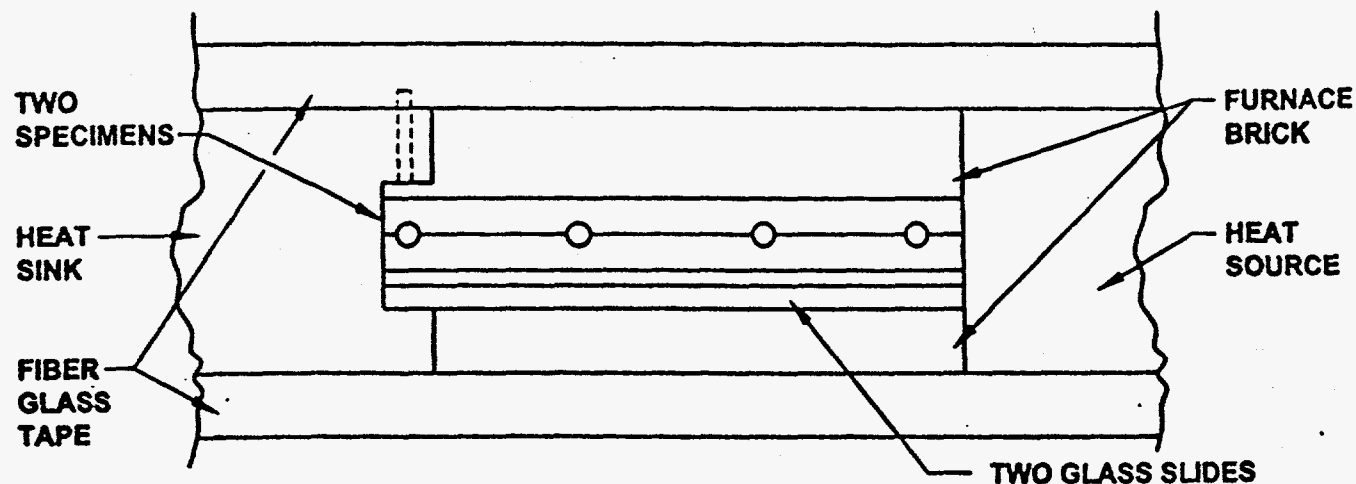
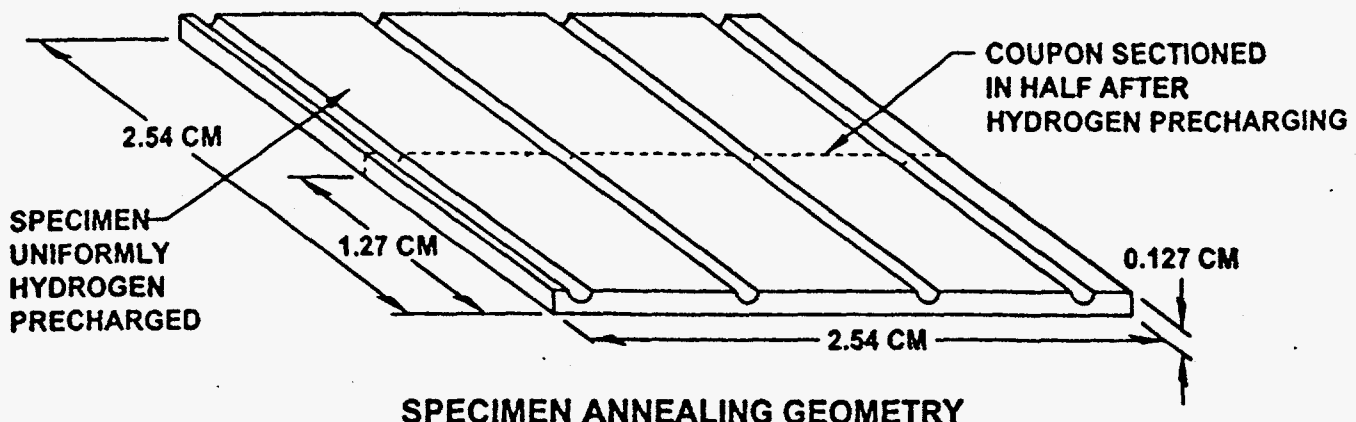


Figure 16 Hydride Dissolution Solvus of Zirconium Alloys as a Function of Temperature



SECTIONING OF SAMPLE FOR HYDROGEN ANALYSIS

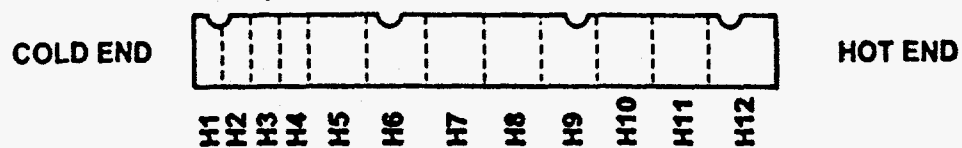


Figure 17 Schematic of the Linear Thermal Gradient Tests

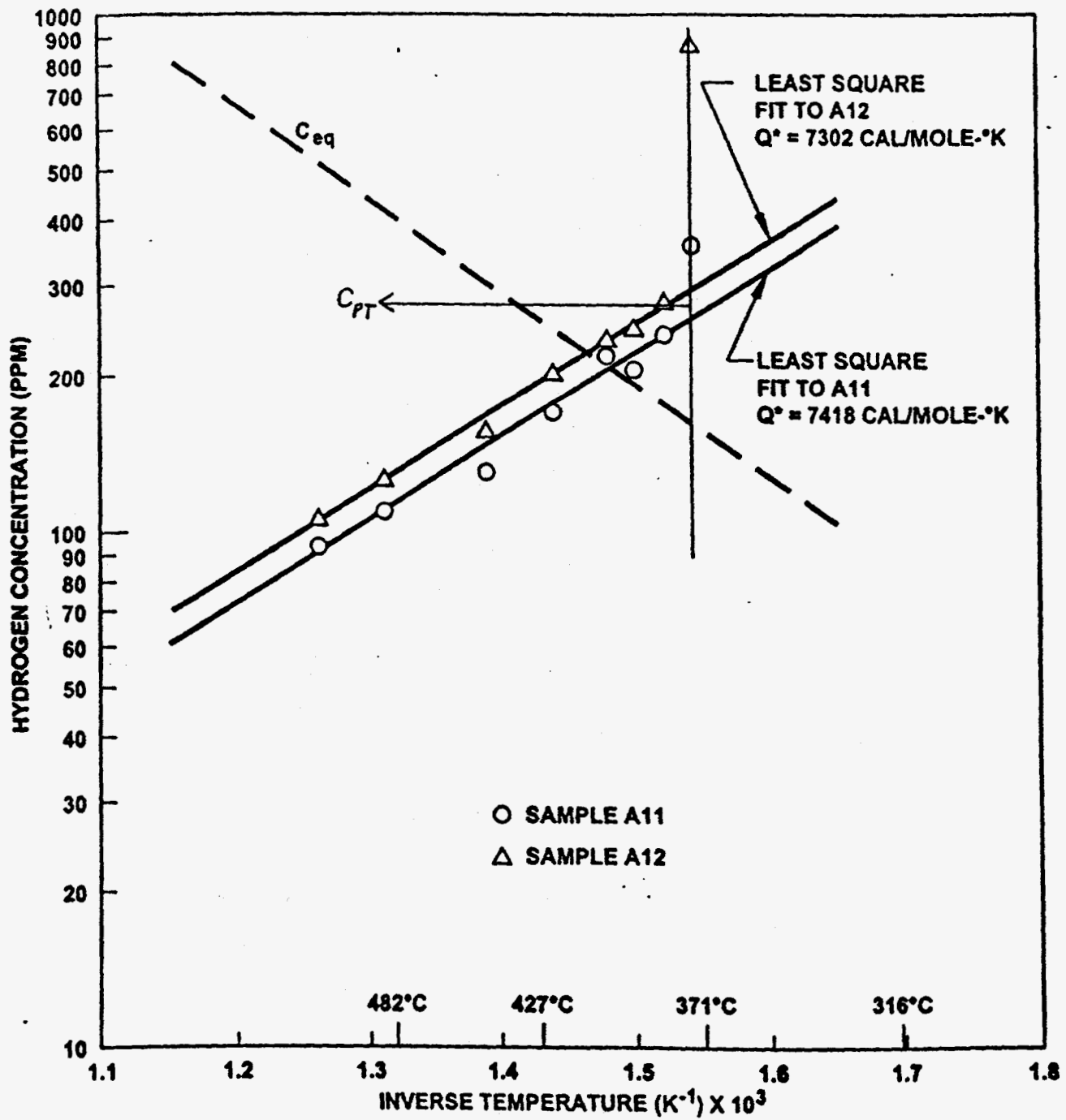


Figure 18 Hydrogen Concentration as a Function of Temperature in a $66^\circ\text{C}/\text{cm}$ Linear Thermal Gradient Test, Cold end at 371°C

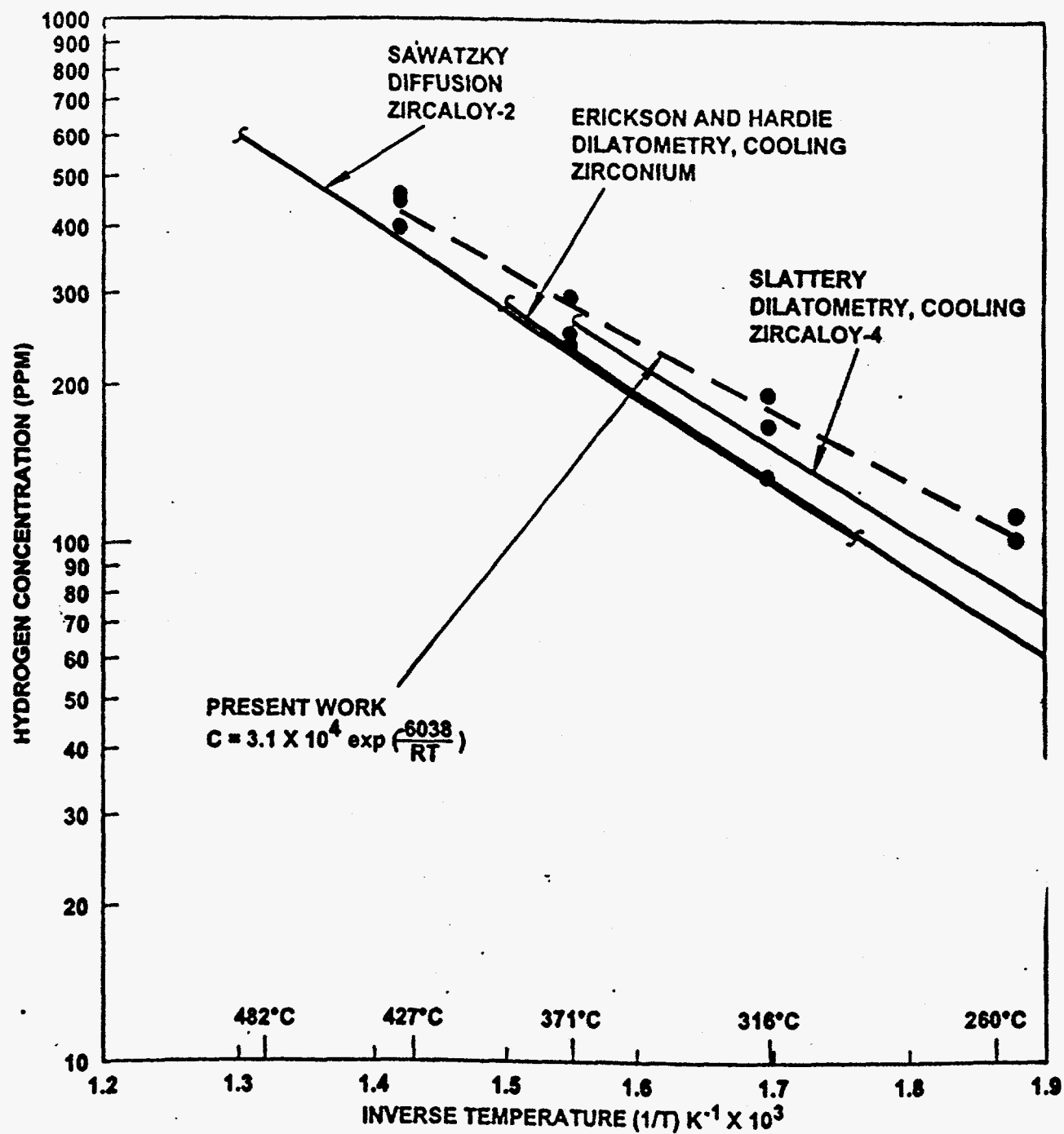
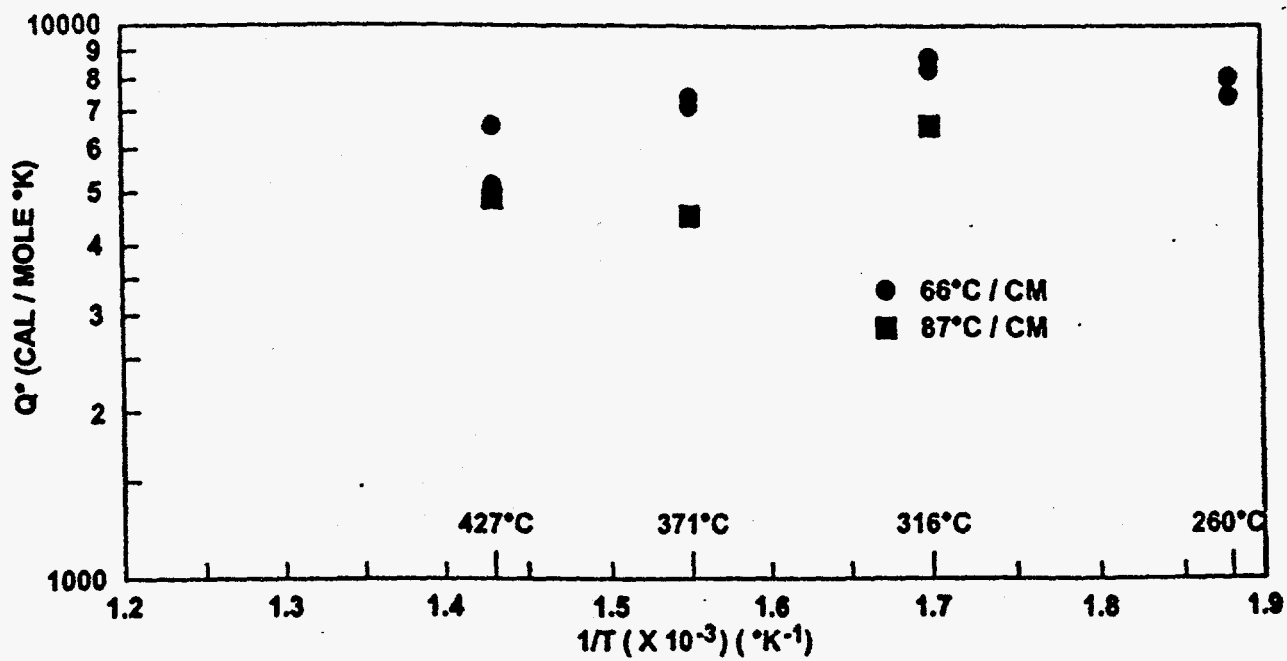


Figure 19 Hydrogen Precipitation Solvus of Zirconium Alloys as a Function of Temperature



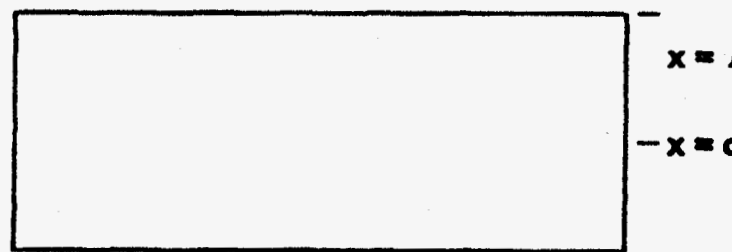
NOTED TEMPERATURE IS COLD TEMPERATURE IN SAMPLES CONTAINING LINEAR THERMAL GRADIENTS OF 300°F / INCH AND 400°F / INCH

Figure 20 Heat of Transport of Hydrogen in Alpha-Annealed Zircaloy-4 as a Function of Temperature

SUPERCHARGING OF ISOTHERMAL CORROSION COUPONS REF. (28)

J_o CONSTANT

C_o CONSTANT



$$M_{\text{ppm}} = \frac{J_o t l \alpha}{D^{1/2}} \cdot \frac{\cosh(\frac{\alpha x}{D^{1/2}})}{\sinh(\frac{\alpha l}{D^{1/2}})}$$

J_o = SURFACE HYDROGEN FLUX

D = DIFFUSION COEFFICIENT

l = SPECIMEN HALF THICKNESS

x = DISTANCE FROM MIDPLANE

M = QUANTITY OF HYDROGEN PRECIPITATED

$$Mx_1/Mx_o = \text{Cosh}(\alpha x/D^{1/2})$$

Figure 21 Method Used to Determine the Precipitation Rate Parameter α

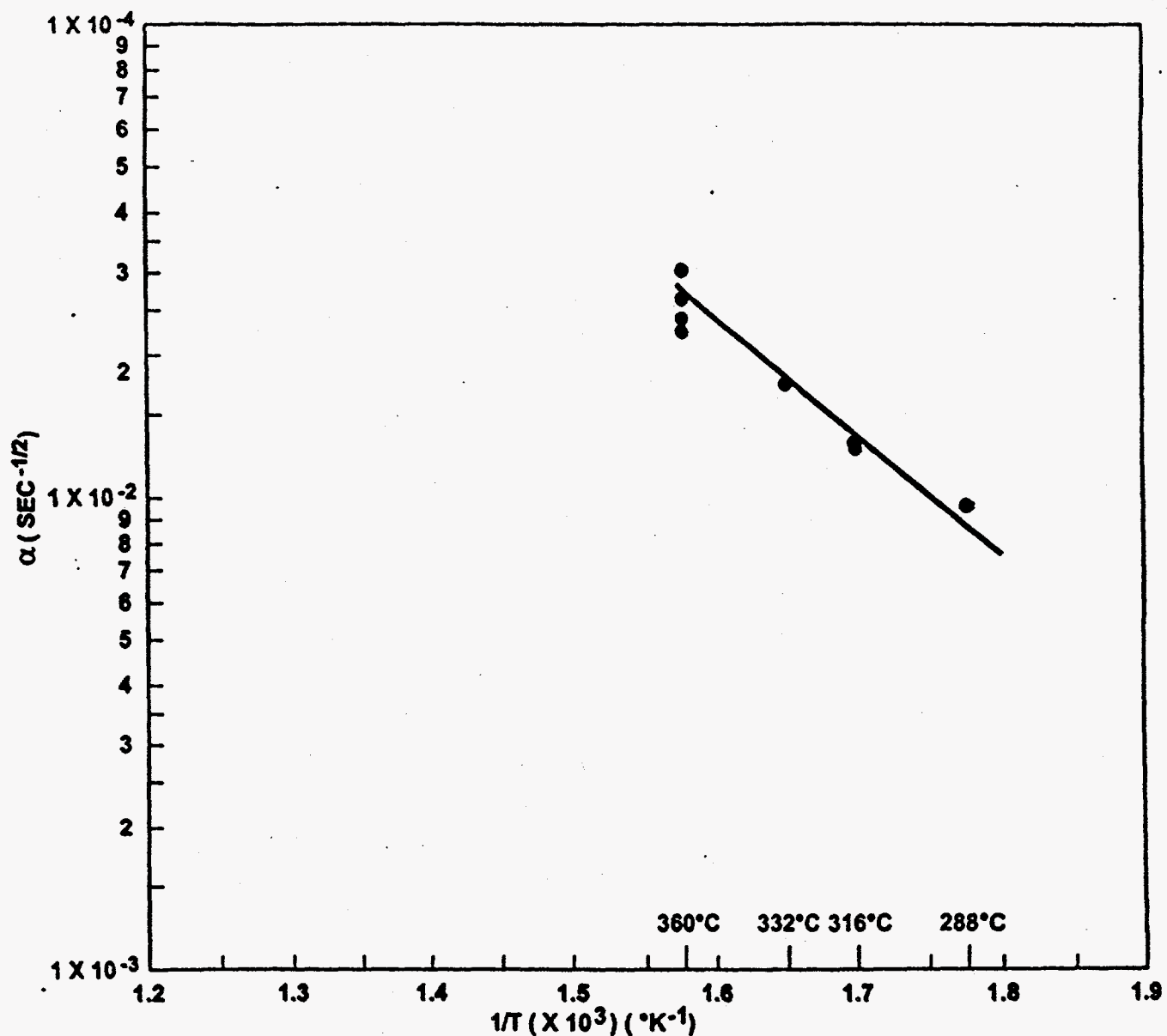


Figure 22 Precipitation Rate Parameter α as a Function of Temperature

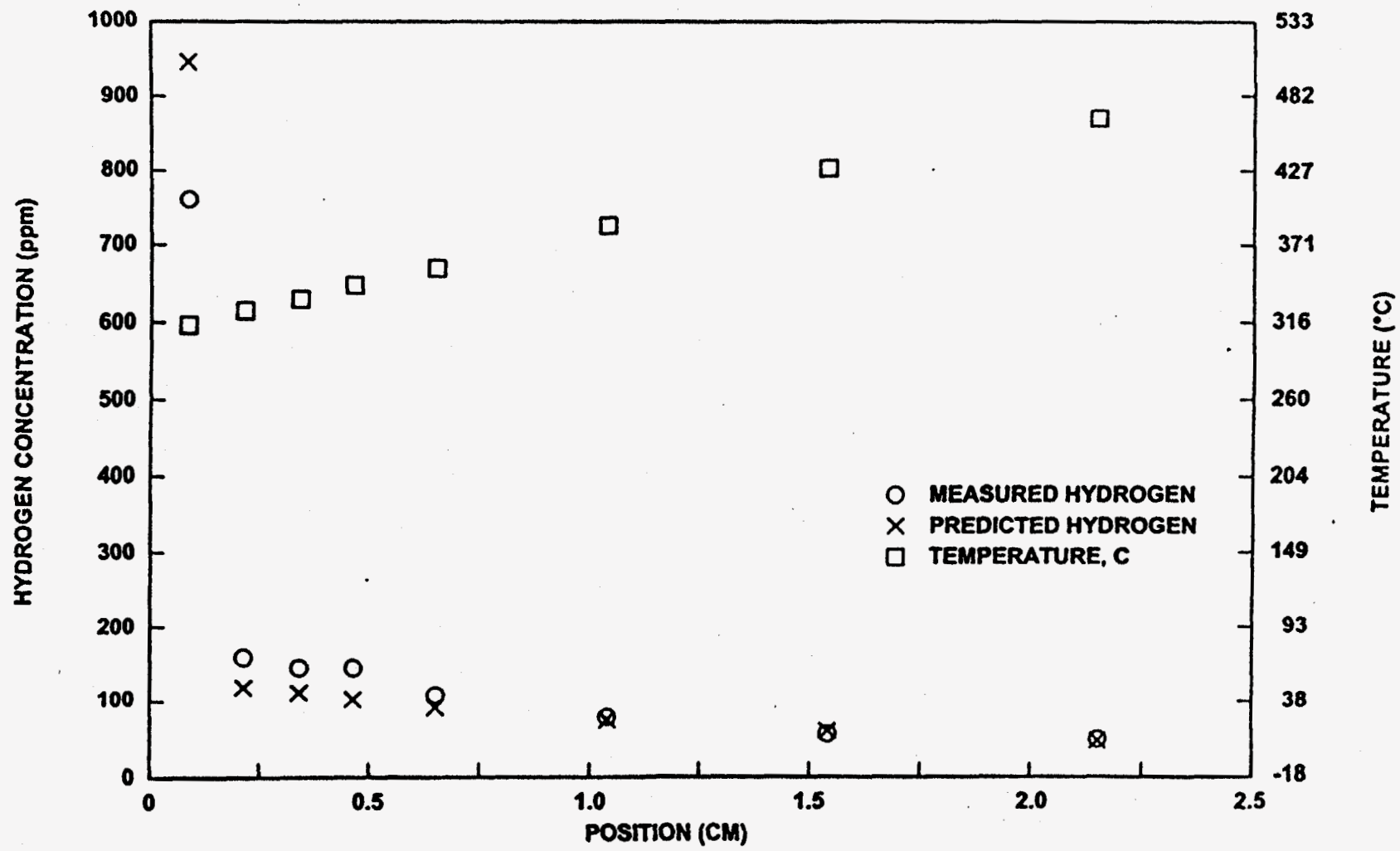


Figure 23 Predicted and Observed Hydrogen Concentration Profile After 30 Days in a Thermal Gradient

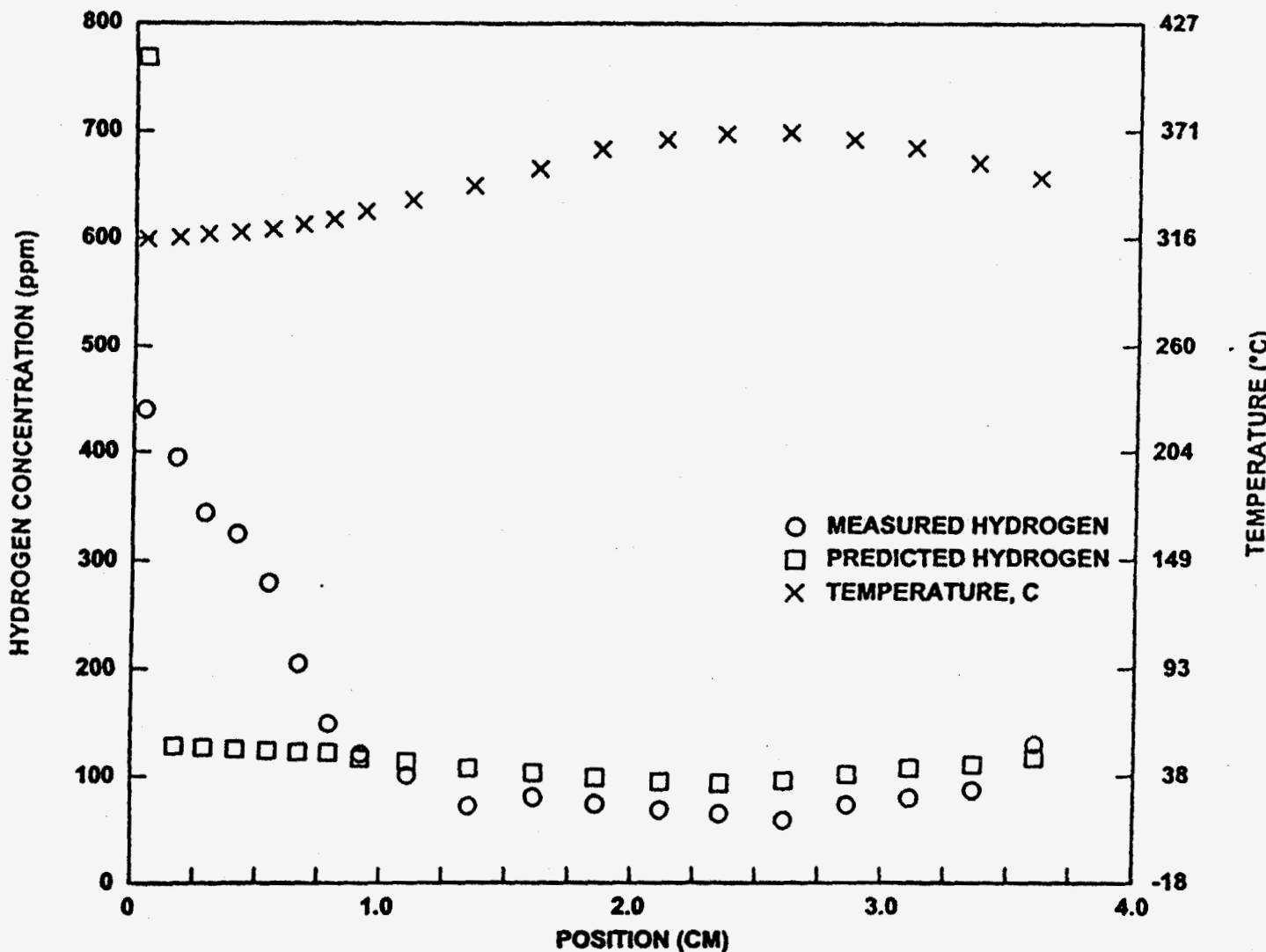


Figure 24 Predicted and Observed Hydrogen Concentration Profile After 200 Days in a Thermal Gradient, Effect on an Internal Temperature Maximum